

Chapter 2

Lanthanide Single-Ion Molecular Magnets

Abstract The most important lanthanide single-ion molecular magnets (SIMMs) reported to date including the lanthanide phthalocyanine, lanthanide β -diketone, and organometallic lanthanide systems are systematically investigated in this chapter. In particular, some important relationships between the structural features and magnetic performances are discussed in detail based on the theoretical results, presenting a guideline for the effective design of lanthanide SIMMs.

Keywords Single-ion molecular magnet • Quantum tunneling • Uniaxial anisotropy • Phthalocyanine • β -diketone • Organometallic

Over the past few years, molecular magnetic materials have flourished and ranged from the pioneering 2D/3D magnetic networks [1, 2] to 1D single-chain magnets (SCMs) [3, 4], 0D polynuclear metal [5] and metal-radical [6, 7] SMMs, and finally the smallest magnet-like molecules including only one single magnetic ion usually called single-ion magnet (SIM) [8–10]. In particular, the development of the latter class of molecules, i.e., SIMs, has been one of the hottest topics in SMM research in recent years, the reason for which is that their simple structure compared with polynuclear complexes allows us to have a better understanding for the correlation between structures and magnetic properties and further to fine-tune their SMM properties [10]. As mentioned in Chap. 1, to avoid misleading the readers from other research fields, we use the term single-ion molecular magnet (SIMM) in the following sections. The first example of such nanomagnets was reported by Ishikawa et al. in 2003 in a family of complexes of general formula $[\text{LnPc}_2]^-$ with a “double-decker” structure [11], where the Tb species demonstrates a high effective barrier, $U_{\text{eff}} = 230 \text{ cm}^{-1}$, far surpassing that of Mn_{12} SMM. This discovery further stimulated the successful design of a growing number of lanthanide SIMM systems, the most typical examples being lanthanide pol-yoxymetalates (LnPOM) [12], lanthanide β -diketone [8, 13], and organometallic double-decker [9, 14] lanthanide complexes. It is noteworthy that, recently, the SIMM family has been extended into the mononuclear *d*-transition metal [15–17]

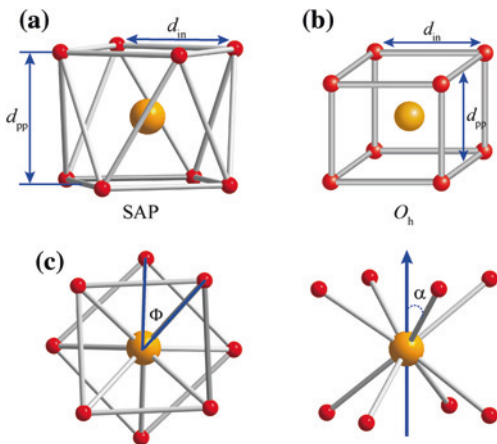
and actinoid [18, 19] complexes with several successful examples being achieved. Nevertheless, to date it is still heavily dominated by lanthanide-based SIMMs, where not only the complexes with high axial symmetry behave as the effective SMMs [11, 20, 21], but also the magnetic relaxation behavior can be observed in some low-symmetry lanthanide complexes [9, 22], mainly because the strong internal single-ion anisotropy of lanthanide ion arising from the large unquenched orbital angular moments greatly facilitates the design of SIMMs, while the subordination of the crystal field to the spin–orbit interaction makes it a minor factor in the overall electronic structure [23]. However, our goal is not to simply synthesize such magnetic molecules, but to achieve a SMM with high effective barrier and blocking temperature and retain its functionality in a more readily accessed temperature regime. Therefore, the role of crystal field must be highlighted, because a suitable crystal field is of critical importance in producing the electronic structure requisite for strong single-molecule magnets, which can be seen in the simple model developed by Long in Chap. 1 [23]. In particular, the effect is very sensitive in SIMMs, where a minor structural alteration may lead to drastic effects on the magnetism. For example, *ab initio* calculations show that the changes of the coordinated water molecule—removal of the water molecule and the positioning of hydrogen atoms—have great impact on the orientation of the anisotropy axis in Dy-DOTA complex [24, 25]. In addition, the impact of ligand donor strength within a given coordination geometry was also explored recently by Long through comparing two isostructural trigonal prismatic complexes with pyrazolate and N-heterocyclic carbene ligands, respectively [26]. The results reveal that, like molecular symmetry, ligand-donating ability is a variable that can be controlled to the advantage of the synthetic chemist in the design of SMMs with enhanced relaxation barriers. As a result, it is of vital importance to fine-tune the interaction between the single-ion electron density and the crystal field environment to make the magnetic moment of individual ion in a SIMM to be blocked as efficient as possible [23]. In this chapter, we focus on the synthetic strategies developed from the synthetic chemists providing a tailored chemical environment to modify the crystal field around lanthanide ion and the theoretical interpretations for magnetism from theoreticians, aiming at better guiding the SIMM design and finally obtaining highly effective SMMs.

2.1 Single-Ion Anisotropy and QTM

In SIMMs where magnetic exchange interactions are absent, the uniaxial anisotropy requisite for strong SMM behavior is mainly deriving from two aspects, one being single-ion contribution from unquenched first-order orbital moments and the other being crystal field contribution. In contrast to transition metal ions, a preeminent feature of lanthanide ions in the design of SIMM is their inherent strong single-ion contribution to anisotropy from the unquenched orbital moments and strong spin–orbital coupling interactions [27, 28], which provide a foundation to

achieve a strongly uniaxial anisotropy necessary for the magnetic moment of individual ions in molecule to be blocked. Further, crystal field turns out to be more crucial factor in making the best of the inherent anisotropy to obtain a robust SMM [23]. As stated in the model of J.R. Long in Chap. 1, a suitable crystal field can effectively enhance the single-ion anisotropy of lanthanide ions and further stabilize the high-magnitude m_J as ground state, which provides the underlying conditions to achieve a SMM. Here, a great number of the reported lanthanide SIMMs have indicated that it is easy to obtain a SIMM using a lanthanide ion, especially the Dy ion whose large magnetic moment and odd-electron configuration make it the most prolific lanthanide ions to date [29]. Nevertheless, it must be stressed that the fast QTM under zero-dc field occurs in most lanthanide SIMMs, especially in the low-symmetry complexes, as evidenced by the butterfly-shaped magnetic hysteresis and the rapidly increasing χ'' components with the decreasing of temperature in χ'' versus T plots [8, 13]. The presence of such fast QTM is very unfavorable to enhancing their SMM properties and the coercive fields (H_c) in the hysteresis loops denoting the strength of a magnet can be significantly reduced [20]. The transversal anisotropic components (g_x, g_y) in Kramers ions or the intrinsic tunneling gap (Δ_{tun}) in non-Kramers ions is the main factor that induces QTM and is extremely sensitive to the asymmetric factors in the structure of mononuclear complexes [30]. In addition, the intermolecular magnetic interactions and the hyperfine interactions between the electron and nuclear spins are also important sources of QTM in lanthanide SIMMs [11, 31]. To suppress the QTM, a series of measures can be adopted, such as applying a dc magnetic field on samples [8], measuring the dynamic properties of frozen solution [32], and magnetic dilution, but the most important is to modify the local crystal field around the lanthanide ions to improve single-ion anisotropy while reducing the g_x and g_y or Δ_{tun} . Here, an important superiority of mononuclear lanthanide magnets is their tenability [33], which allows for increased control over crystal field, and therefore magnetic properties, when compared to multinuclear species. Therefore, alongside the remarkable synthetic and theoretical progresses has come the development of several ways of achieving a high degree of axiality of single-ion anisotropy. One way is to achieve only one very strong chemical bond with the metal ion, which dominates over all other chemical bonds of the metal site, leading to the intrinsically axial nature of the total ligand field felt by the metal center [20]. To date, only a handful of such examples were discovered, but showing the strongly blocking of magnetization. Typically, the DyNCN complex mentioned in Chap. 1 exhibits the high U_{eff} for the reorientation of the magnetic moment and the particular relaxation path via the second excited state [34], which is still fairly sparse in lanthanide SIMMs. The more conventional route for obtaining the strong single-ion anisotropy is to modify the coordination geometry to reach as perfect an axial symmetry as possible, which is very important in reducing the possible mixing of the m_J levels, further confirming a pure high- m_J state as ground state [35]. Here, according to strict group-theoretical rules, an ideal axial symmetry can be achieved in point groups $C_{\infty v}$, $D_{\infty h}$, S_8 , D_{4d} , D_{5h} , D_{6d} , which show the vanishing off-diagonal crystal field parameters B_k^q ($q \neq 0$) responsible for generating the mixing m_J levels [36].

Fig. 2.1 Schematic structures of SAP (a) and cubic (b) geometries. (c) The relevant angular parameters in SAP geometry: Φ , the angle between the diagonals of the two squares (*skew angle*); α , the angle between the C_4 axis and a RE–L direction

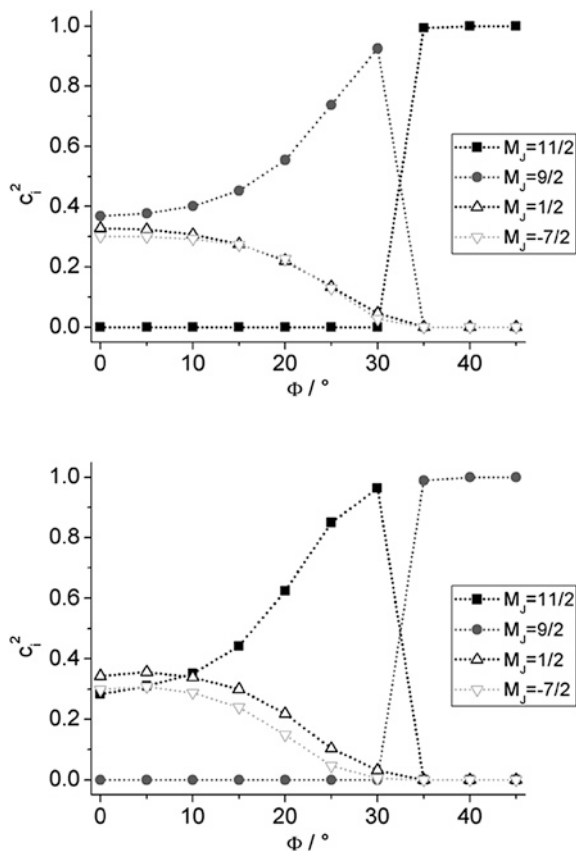


In fact, a great number of SIMM examples with such coordination geometries have been reported, showing very high energy barriers. Here, we take the example of the well-known square antiprismatic (SAP) geometry (D_{4d}), highlighting the key geometrical parameters in the definition of the electronic structure of the metal ion [35, 37], which directly affect the SMM performance.

The SAP geometry has been shown in Fig. 2.1 with several important parameters being labeled. The relevant geometrical parameters are d_{pp} , the distance between the L4 squares; d_{in} , the shorter L–L distance in the L4 square; Φ , the angle between the diagonals of the two squares (*skew angle*); and α , the angle between the C_4 axis and a RE–L direction. Eight identical RE–L distances define the highest symmetry D_{4d} corresponding to $d_{pp} = d_{in}$, $\Phi = 45^\circ$ and $\alpha = 54.74^\circ$, i.e., an axially non-distorted antiprism. Here, the D_{4d} symmetry ($\Phi = 45^\circ$) is taken as a distorted case of the O_h symmetry ($\Phi = 0^\circ$) when the two squares are staggered (Fig. 2.1). The deviation of Φ from 45° will result in the disappearance of D_{4d} symmetry, thus leading to the presence of nonzero B_4^4 and B_6^4 crystal parameters and further an extensive mixing of functions with different m_j values, which are of fundamental importance to promote the quantum tunneling of the magnetization in these systems. The simple calculations performed by D. Gatteschi demonstrate the great impact of a variation of angle Φ on the electronic structure of metal ions due to the introduction of nonzero B_4^4 and B_6^4 , as shown in Fig. 2.2, where the first excited state at $\Phi = 45^\circ$ for the SAP becomes the ground state for distortions of about 15° from pure SAP geometry [35]. The effects are well present in a series of lanthanide β -diketone SMMs showing the enhanced QTM with the deviation of Φ , which will be introduced in the below sections.

Another important factor of affecting the electronic structures of metal ions is the effect of the compression/elongation along the C_4 axis associated with α . Wider α angle corresponds to compression ($\alpha > 54.74^\circ$) and smaller to elongation ($\alpha < 54.74^\circ$) along the tetragonal axis. The main qualitative difference in the calculated parameters is the change of B_2^0 sign on passing from compressed

Fig. 2.2 Variation of the composition of the ground (*top*) and first excited (*bottom*) states on passing from a cube to a square antiprism, calculated by Gatteschi group on the basis of the AOM parameters. Reproduced from Ref. [35] by permission of The Royal Society of Chemistry



to elongated SAP for a given lanthanide ion. For α_J -negative lanthanide ions, Tb^{III} , Dy^{III} , Ho^{III} , Pr^{III} , and Nd^{III} , the B_2^0 sign will change from negative to positive with the variation from elongated to compressed SAP, while the reverse trend is observed in the α_J -positive lanthanide ions, Er^{III} , Tm^{III} , and Yb^{III} , as seen in Fig. 2.3 ($B_2^0 \sim \alpha_J B_0^2$, $\alpha_J < 0$ for Tb^{III} , Dy^{III} et al., while $\alpha_J > 0$ for Er^{III} , Tm^{III} et al.) [38]. Here to achieve a strong SMM, a negative uniaxial anisotropy associated with negative B_2^0 parameters is required to stabilize a high- m_J ground-state doublet. Therefore, the elongated SAP is much more favorable for Dy ion in the design of SMM, and the opposite for Er ion, which is consistent with the real case present in $[\text{LnPc}_2]$ and LnPOM systems.

In this section, we have discussed how to suppress the QTM through enhancing the single-ion anisotropy of lanthanide ions and further take the example of the well-known SAP geometry to show how to fine-tune the local geometry around lanthanide ions favorable for the strong SMM behavior. The following sections focus on the typical lanthanide SIMM systems discovered to date, highlighting their tunability through tailoring their organic ligands, which allows for increased control over structure and therefore magnetic properties.

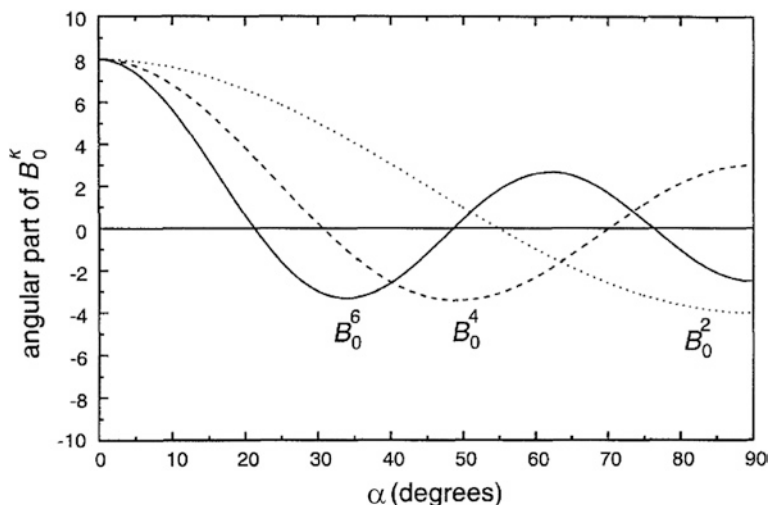


Fig. 2.3 Angular α -dependence of the B_0^k crystal field parameters in a D_{4h} symmetry. It should be noted that the parameter B_0^k in this figure is different from the B_k^0 in the text which contains B_0^k and Stevens equivalent coefficients. Reprinted from Ref. [38]. Copyright 1996, with permission from Elsevier

2.2 [LnPc₂] and LnPOM SIMMs

As seen in Fig. 2.4, both phthalocyanine (Pc) and polyoxometalates (POM) [39] ligands demonstrate the high local symmetry and the rigid characteristic with the coplanar coordinate atoms, which are favorable for the assembly of double-decker sandwich geometry with lanthanide ions ([LnPc₂]). In general, the two coordinate planes are staggered rather than eclipsed, leading to the typical SAP geometry (Fig. 2.1), which thus seems to be very helpful for the design with enhanced SMM properties. In particular, the tunability of substituent groups of Pc ligand (Fig. 2.5) and its redox ability enable us to easily optimize the coordination geometry around lanthanide ions to enhance the single-ion anisotropy as efficient as possible.

2.2.1 Phthalocyanine-Type Ligands and the [LnPc₂] Structure

The phthalocyanine contains four isoindole nitrogen atoms, showing two-dimensional π -conjugated planar structure, which are able to complex with a range of metal ions from transition metal to lanthanide ions [40]. Here, the ionic size and

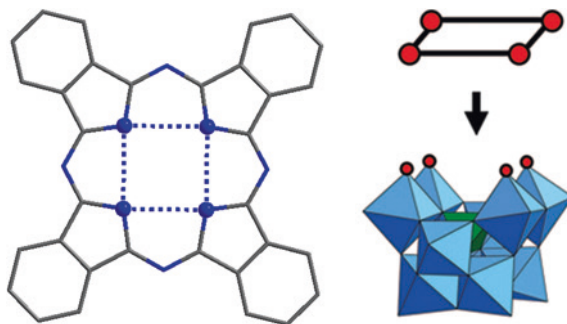


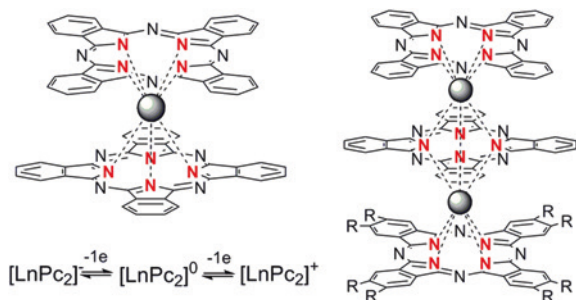
Fig. 2.4 The coplanar coordinate atoms of phthalocyanine (Pc) and polyoxometalates (POM) ligands. Reprinted with the permission from Ref. [39]. Copyright 2010 American Chemical Society

<p>H₂Pc</p>	R ₁ =R ₂ =H	R ₃ =R ₄ =H	Pc
	R ₁ =R ₂ =-OEt	R ₃ =R ₄ =H	Pc-OEt
	R ₁ =R ₂ =-O <i>n</i> Bu	R ₃ =R ₄ =H	Pc-OBu
	R ₁ =R ₂ =-CN	R ₃ =R ₄ =H	Pc-CN
	R ₁ =R ₂ =-CF(CF ₃) ₂	R ₃ =R ₄ =F	Pc-CF
	R ₁ =R ₂ =R ₃ =H	R ₄ =OCH(C ₂ H ₅) ₂	Pc-OC5
	R ₁ =R ₂ =-OC ₁₂ H ₂₅	R ₃ =R ₄ =H	Pc-OC12
	R ₁ =R ₂ =-OPh- <i>p</i> - <i>t</i> Bu	R ₃ =R ₄ =H	Pc-OPh
	R ₁ = <i>t</i> Bu	R ₂ =R ₃ =R ₄ =H	Pc-Bu
	R ₁ =R ₂ = -OCH ₂ CHO(CH ₂) ₁₁ CH ₃ CH ₃	R ₃ =R ₄ =H	Pc-ODOP
<p>R = (TPP)</p>	<p>R₁ R₂ = </p>	R ₃ =R ₄ =H	Pc-IPD
<p>R = Cl (TCIPP)</p>			
<p>R = Cl (TCIPP)</p>			
<p>H₂tmtaa</p>	<p>R₁ R₂ = </p>	R ₃ =R ₄ =H	Pc-a Pc-b Pc-c

Fig. 2.5 Phthalocyanine (Pc) ligands with different substituent groups and the ligands showing the similar structure to Pc ligand used in lanthanide SIMMs

valence of metal ion is a critical factor in determining the structure of coordinate complexes. Pc and divalent 3*d* transition metal ion such as Mn²⁺, Fe²⁺, Ni²⁺, and Cu²⁺ can form planar molecules with no axial ligand [41], while the double-decker and even triple-decker sandwich-type structures (Fig. 2.6) are supported in the lanthanide phthalocyanine complexes with the increasing ion radius. It is noteworthy that various crystalline forms of bis(phthalocyaninato) lanthanide

Fig. 2.6 Schematic structures of double-decker and triple-decker sandwich-type structures with Pc ligands

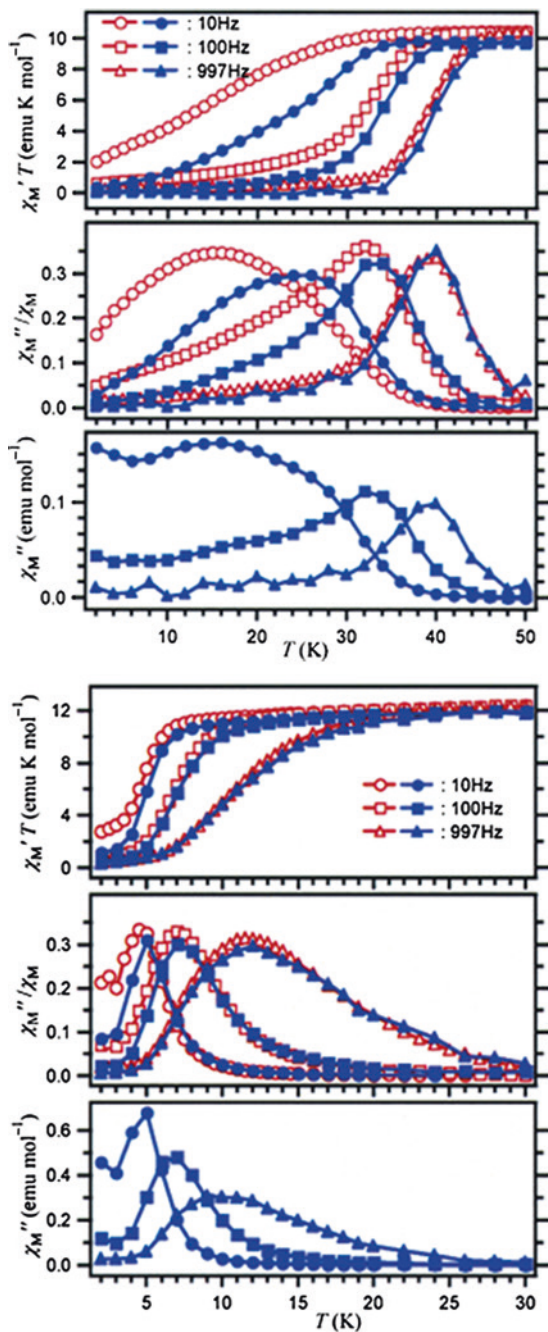


double-decker complexes including neutral, cationic, and anionic species can be obtained by controlling a redox reaction on the ligand side (Fig. 2.6), which thus allow us to better modulate the electronic structure of the complex and further control their dynamic magnetism without introducing any additional magnetic site or spin system [42]. Importantly, a great number of phthalocyanine derivatives are obtained through substituting some or all of the hydrogen atom(s) of the benzene rings, as seen in Fig. 2.5. The various modifications of substituent groups in Pc ligand provide a good condition for exploring the relaxation dynamics of different $[\text{LnPc}_2]$ species and isolating lanthanide SMM with high effective barrier.

2.2.2 The Magnetism of Seminal $[\text{LnPc}_2]^- \cdot \text{TBA}^+$

The early research interest of lanthanide phthalocyanine complexes can date back to 1960s [40], but the exploration for their SMM properties was just started in 2003 [11], when Ishikawa firstly demonstrated phthalocyanine Tb^{III} and Dy^{III} complexes functioning as magnets at the single-molecular level. Their structures have been well established by the prior investigations, showing an elongated SAP with $d_{\text{pp}} > d_{\text{in}}$ [43]. Importantly, the consistent binding mode of the phthalocyanine macrocycles to lanthanide metal center leads to the very small deviation from the SAP symmetry in the first coordination sphere for the late lanthanide ions with smaller ion radii. Such a high symmetry SAP is favorable of an isolated ground-state doublet with the large m_J value well separated in energy from the first excited state, necessary for achieving a high-performance SMM, for the lanthanide ions with oblate electron density such as Tb^{III} , Dy^{III} , and Ho^{III} in spite of the non-Kramers ion properties of Tb^{III} and Ho^{III} ions. Figure 2.7 shows ac magnetic susceptibilities as a function of temperature of polycrystalline powder sample of $[\text{LnPc}_2]^- \cdot \text{TBA}^+$ ($\text{Ln} = \text{Tb}^{\text{III}}$ and Dy^{III} , $\text{TBA}^+ = (\text{C}_4\text{H}_9)_4\text{N}^+$) [11]. The maximum of χ''/χ_{dc} , typical feature of SMM behavior, was observed at 15, 32, and 40 K with ac frequency of 10, 100, and 997 Hz, respectively, for undiluted Tb complex. In the diluted samples in diamagnetic $[\text{YPc}_2]^- \cdot \text{TBA}^+$, the shifts to

Fig. 2.7 The ac susceptibility data of Tb (*top*) and Dy (*bottom*) complexes in [LnPc₂]⁻·TBA⁺, with the open marks for the undiluted samples and the filled marks for the diluted samples. Reprinted with the permission from Ref. [11]. Copyright 2003 American Chemical Society



higher temperature of χ''/χ_{dc} peaks clearly indicate that slow relaxation of magnetization is single-molecule origin. In addition, it is remarkable that the Tb^{III} complex demonstrates the higher blocking temperature than Dy^{III} analogue, as seen in Fig. 2.7, which could be directly associated with their distinct electronic sublevel structures of the ground-state multiplets of the complexes discussed in the following sections.

For lanthanide phthalocyanine complexes, the fluorescence and absorption spectra associated with lanthanide centers are unavailable in obtaining the sublevel structures of the ground-state multiplet, because the low-lying Pc-centered energy levels quench the lanthanide fluorescence and the extremely intense Pc-centered absorption bands conceal the lanthanide-centered bands. In 2003, Ishikawa et al. determined their sublevel structures using a simultaneous fitting of paramagnetic NMR shifts and magnetic susceptibility data by the set of LF parameters from a multidimensional nonlinear minimization algorithm. Figure 2.8 shows the theoretical and observed $\chi_m T$ values and paramagnetic shifts ($\Delta\delta$) of the ¹H NMR signal, and substructures of the ground multiplets [44]. Here, the energy diagram for the ground multiplets (Fig. 2.8c) reveals that the Tb^{III}, Dy^{III}, and Ho^{III} complexes possess the well-isolated ground-state doublet with large m_J values, which are favorable of the presence of their SMM behaviors. In particular, the Tb complex shows the ground state with largest m_J values and a separation of more than 400 cm⁻¹

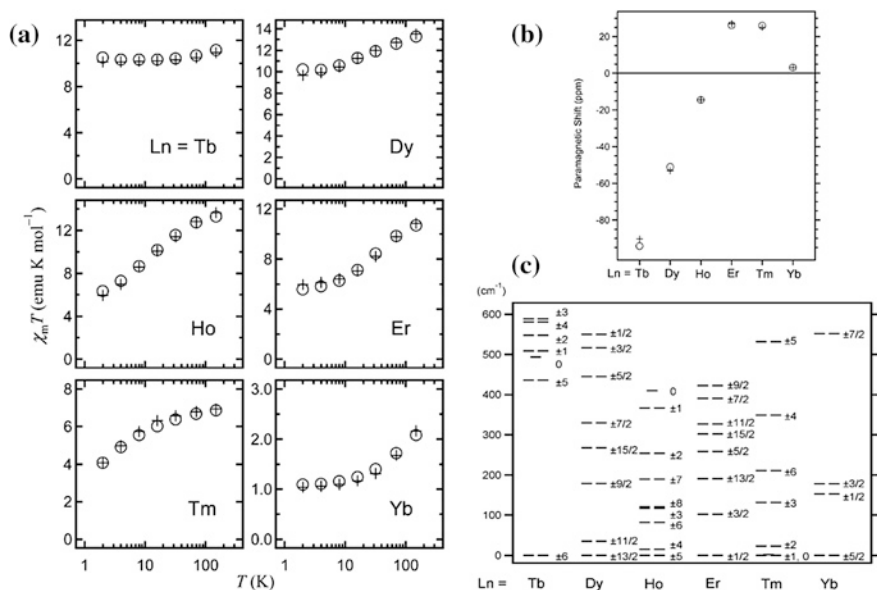


Fig. 2.8 **a** The comparisons of theoretical and experimental temperature dependence of the $\chi_m T$ values. **b** The theoretical and experimental paramagnetic shifts of the ¹H NMR signal of the α -proton on the Pc ligands. **c** The obtained energy diagram for the ground-state multiplets. Reprinted with the permission from Ref. [44]. Copyright 2003 American Chemical Society

between the ground state and the first excited state, which are well in agreement with its very high effective barrier of 230 cm⁻¹ surpassing several times of that of Mn₁₂ SMM. In the Dy complex, the ground state shows the quantum number of $m_J = \pm 13/2$ larger than that of the first excited state ($m_J = \pm 11/2$), still suggesting the strong Ising-type anisotropy, even though the doublet substates with the largest m_J do not lie in the lowest state. Here, the separation of 35 cm⁻¹ between the ground state and the first excited state is close to the effective energy barrier (28 cm⁻¹) determined experimentally in the diluted samples of Dy complex, suggesting that relaxation will take place by thermal-activated quantum tunneling through the first excited state. In addition, for the Er and Tm complexes the state with the smallest quantum number lies in the lowest energy states, indicating the easy-plane anisotropy, thus leading to the disappearance of SMM behavior.

Another important characterization for SMM is the observation of hysteresis loops. In known transition metal SMMs, the stepwise hysteresis loop was usually observed at low temperature, which is mainly ascribed to the QTM allowed by the avoided level crossing of different electronic levels m_S under an appropriate magnetic field [45]. Here, the Tb^{III}, Dy^{III}, and Ho^{III} complexes also show the staircase-like hysteresis loops at the relatively low magnetic field [31, 46], but it seems to be insufficient to explain them through the simple level crossing of different m_J states, because the separations between two adjacent m_J states are so high, up to a few hundred wave numbers surpassing that of transition metal cluster by an order of magnitude, that such level crossings occur only at very high fields. Therefore, Ishikawa et al. applied the new theoretical model with the nuclear spins terms to successfully explain the step structures of hysteresis observed around nonzero magnetic fields [31].

$$H_{Ln} = H_{LF} + \mu_B(\mathbf{L} + 2\mathbf{S}) \times \mathbf{H} + A_{hf} \mathbf{J} \times \mathbf{I} + P \left\{ I_z^2 - 1/3I(I+1) \right\}$$

$$H_{LF} = A_2^0 \langle r^2 \rangle \alpha O_2^0 + A_4^0 \langle r^4 \rangle \beta O_4^0 + A_4^4 \langle r^4 \rangle \beta O_4^4 + A_6^0 \langle r^6 \rangle \gamma O_6^0 + A_6^4 \langle r^6 \rangle \gamma O_6^4$$

For H_{Ln} , the H_{LF} , \mathbf{L} , and \mathbf{S} are operator equivalents of the LF potential on the f -system, orbital angular momentum, and spin angular momentum operators, respectively. The third and fourth terms represent the hyperfine and nuclear quadrupole interactions, respectively, in which the A_{hf} and P are coupling constants. The interactions between the $4f$ electrons and the nucleus spin lead to a $[(2J+1)(2I+1) \times (2J+1)(2I+1)]$ matrix. In the case of the Tb complex (Fig. 2.9a, b), terbium possesses a nucleus with $I = 3/2$ spin in a natural abundance of 100 %. The ground-state doublet, $m_J = \pm 6$, splits into eight states denoted as $|m_J\rangle|I_z\rangle$, where $I_z = \pm 3/2$ and $\pm 1/2$. Figure 2.9b shows the Zeeman diagram for the eight states with the $16 = 4^2$ crossing points but only 13 magnetic-field positions, which clearly explains the positions of staircase in the hysteresis loop of diluted [TbPc₂]⁻ samples. In addition, such staircase-like hysteresis loops are also observed in the diluted Dy and Ho samples, as seen in Fig. 2.9c, d, respectively. For the sample containing Ho ions possessing a nucleus with $I = 7/2$ spin in a natural abundance of 100 %, the same explanation

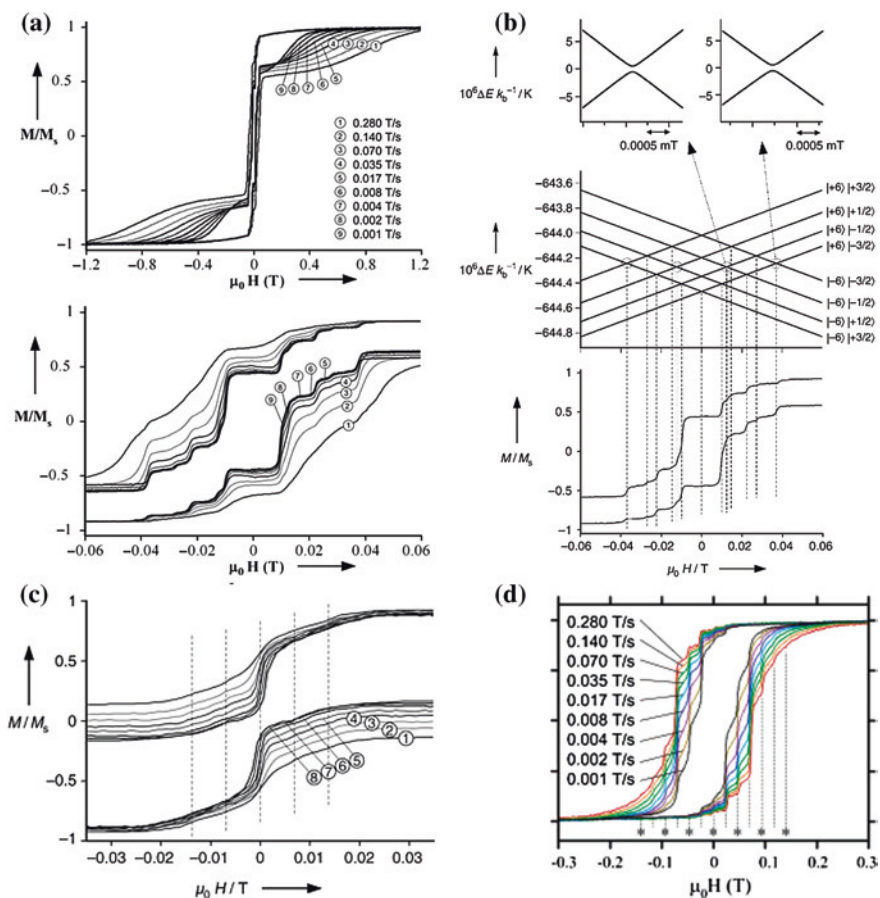


Fig. 2.9 Hysteresis loops at 0.04 K for the Tb (a), Dy (c) and Ho (d) complexes of $[\text{LnPc}_2]^-$. **b** Zeeman diagrams of Tb complex for the lowest $m_J = \pm 6$ substates combined with the $I = 3/2$ nucleus state calculated with the ligand-field parameters. **a–c** Reproduced from Ref. [31] by permission of John Wiley & Sons Ltd. **d** Reprinted with the permission from Ref. [46]. Copyright 2005 American Chemical Society

is given to the observed step positions in its hysteresis loops. However, for Dy there are seven naturally occurring isotopes, showing two different nuclear spins, $I = 0$ and $5/2$. For $I = 0$, no tunneling should occur because of the Kramers theorem of spin parity, while the coupling between $I = 5/2$ and $4f$ electrons leads to an integer total spin and further the avoided level crossings in the Zeeman diagram, which interpret the small step in the hysteresis loops of diluted Dy sample.

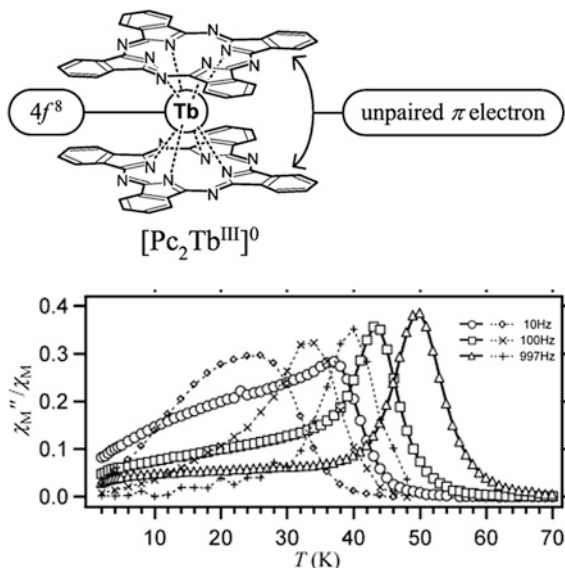
2.2.3 The Enhanced SMMs from the Redox Reactions

In the above section, we discussed the magnetism and electronic structures of the anionic form of bis(phthalocyaninato)terbium, where the Pc ligands have a formal charge of 2- with a closed shell π electronic system. However, it has been well known that one/two-electron oxidation of [LnPc₂]⁻ can occur on the ligand side, resulting in the neutral and cationic [LnPc₂]^{0/+} species (Fig. 2.6), which provide a great platform for studying the modulation of relaxation dynamic by controlling a redox reaction on the ligand side in pursuit of the envisaged SMM properties. In particular, the previous theoretical studies have indicated that the highest occupied molecular orbital (HOMO) and the next HOMO of [LnPc₂]⁻ are the antibonding and bonding linear combinations, respectively, of the highest occupied π orbitals of the component Pc²⁻ ligands [47, 48]. The removal of the two electrons from the HOMO orbital will thus shorten the Pc–Pc distance and the height of the coordination polyhedron of the lanthanide ion, which greatly strengthen the axial component of the ligand field and further lead to the possibly enhanced SMM behavior [49]. In fact, such several typical examples have been reported by Ishikawa and other groups, showing the significant increase of the barrier energy for magnetization reversal from the redox reaction on the ligand side.

In 2004, Ishikawa et al. reported the first example of π -radical [TbPc₂]⁰ SMM from the ligand oxidation of the anionic [TbPc₂]⁻ complex, which generates one unpaired π electron delocalized over two Pc ligands (Fig. 2.10) [49]. Clearly, the peaks of the out-of-phase component of the ac susceptibility are shifted to significantly higher temperatures in contrast to the values of the anionic complex, as seen in Fig. 2.10. Here, the effective barrier can be extracted to be 410 cm⁻¹, which is more than 100 cm⁻¹ higher than that of the seminal complex, indicating thus the enhanced SMM behavior. In order to eliminate the effect of intermolecular interactions, the peripheral H atoms of Pc ligands are substituted by the long-chain alkoxy groups in the [TbPc₂]⁰ complex, which can effectively increase the intermolecular distances and thus reduce the intermolecular interactions. Therefore, the ac susceptibility of [Tb(Pc-OC12)₂]⁰ in a frozen solution of eicosane shows the similar temperature range, where slow relaxation of magnetization is observed, to the [TbPc₂]⁰ complex, indicating that the magnetic relaxation phenomena is single-molecule origin, rather than resulting from intermolecular interactions and long-range magnetic order.

In 2007 and 2008, the cationic Tb and Dy phthalocyanine complexes arising from the two-electron oxidation of its corresponding anionic complexes were subsequently investigated by Ishikawa et al. [42, 50]. Here, the essential modifications for the seminal complex [LnPc₂]⁻ should be performed due to the extremely low solubility of [LnPc₂]⁺ to organic solvents. The substituted Pc-OEt ligand, 2,3,9,10,16,17,23,24-octaethoxyphthalocyanine, turns out to be effective in increasing the solubility of the cationic complex [LnPc₂]⁺ to organic solvents. Therefore, the cationic complex [Ln(Pc-OEt)₂]⁺(SbCl₆)⁻ (Ln = Tb and Dy) was isolated by oxidizing their neutral complexes with phenoxathiinium

Fig. 2.10 The schematic structure (*top*) and ac susceptibility data (*bottom, solid lines*) of π -radical $[\text{TbPc}_2]^0$. Dotted lines represent the ac susceptibility data of $[\text{TbPc}_2]^-$. Reprinted with the permission from Ref. [49]. Copyright 2004 American Chemical Society



hexachloroantimonate in dichloromethane. The changes of coordination geometry are demonstrated at the top of Fig. 2.11, showing a longitudinal contraction of the SAP polyhedron relative to the anionic complexes, which are predicted by DFT theoretical calculations. Comparing the alternating current (ac) susceptibility data of the cationic and the corresponding anionic complexes at the bottom of Fig. 2.11, we can see that the χ'' peaks clearly shift to the higher temperature, indicating the enhanced slow relaxation process. For the cationic Tb and Dy complexes, the χ'' peaks at 1000 Oe were observed at 52 and 25 K, which are 12 and 15 K higher than that of their anionic complexes, respectively. Naturally, their anisotropy barriers for the spin reversal of magnetization show also a corresponding increase. Here, the effective barrier of $[\text{Tb}(\text{Pc}-\text{OEt})_2]^+$ was estimated by Arrhenius analysis to be 550 cm^{-1} , showing an 8 % increase in contrast to that of the anionic complex [42]. More strikingly, the cationic Dy complex shows a 55-cm^{-1} effective barrier, about twice as large as that of its anionic complex, and the hysteresis loop at 1.8 K exhibits a large remnant magnetization at zero field [50]. The observations of the dynamic magnetism presented here are consistent with the longitudinal contraction of the SAP polyhedron, which is expected to increase the ligand-field splitting of the ground multiplet of lanthanide ions and further leads to the blocking of magnetic moments at higher temperature.

In addition, magnetic circular dichroism (MCD) spectroscopy was applied to further probe the magnetic properties of three interconvertible redox states in a family of new lanthanide phthalocyanine complexes, $[\text{Ln}(\text{Pc}-\text{IPD})_2]^{-/0/+}$ [51]. The MCD spectroscopy, showing a high sensitivity compared to the conventional

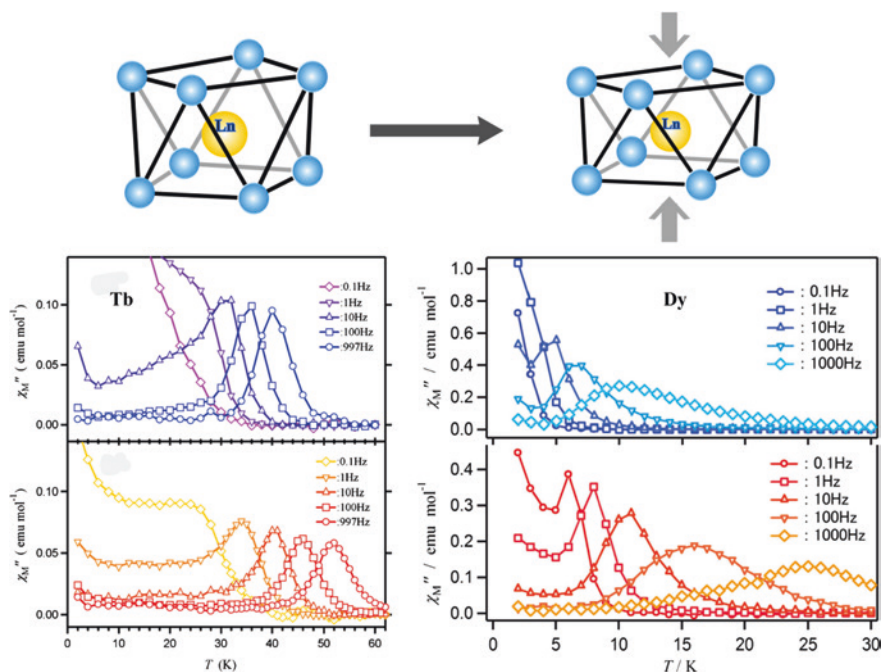


Fig. 2.11 Schematic diagram of the contraction of the coordination space and the changes of magnetic dynamics upon two-electron oxidation from [LnPc₂]⁻ to [LnPc₂]⁺ (Ln = Tb and Dy). Reprinted with the permission from Refs. [42, 50]. Copyright 2007 and 2008 American Chemical Society

magnetometer, has been viewed as a powerful tool for the optical detection of the magnetic behavior [52]. The field-dependent MCD intensity was recorded at 705, 664, and 631 nm for three samples as solutions in CH₂Cl₂ with 0.8 M [NBu₄][BF₄], as seen in Fig. 2.12 [51]. Therefore, the butterfly-shaped hysteresis was observed in both anionic and cationic samples, but the hysteresis of the cationic sample shows a larger coercive field and stronger remnant signal, which indicate that the cationic complex exhibits the larger ligand-field splitting of the ground multiplet and further behaves as a more effective SMM, in agreement with the above results presented by the ac susceptibility measurements. Nevertheless, the field-dependent MCD spectrum of the neutral complex demonstrates the different hysteresis behavior from their ionic complex. Here, the perfect hysteresis loop was observed without the clear steps indicating the QTM relaxation process around 0 T. In results, the neutral complex exhibits the greatest coercive field and least QTM at zero field, suggesting that the neutral complex is better suited to SMM applications.

In 2013, S.M. Gorun et al. firstly reported the magnetic study of the halogenated phthalocyanine double-decker lanthanide complex, [Tb(Pc-CF₃)₂]-H, showing

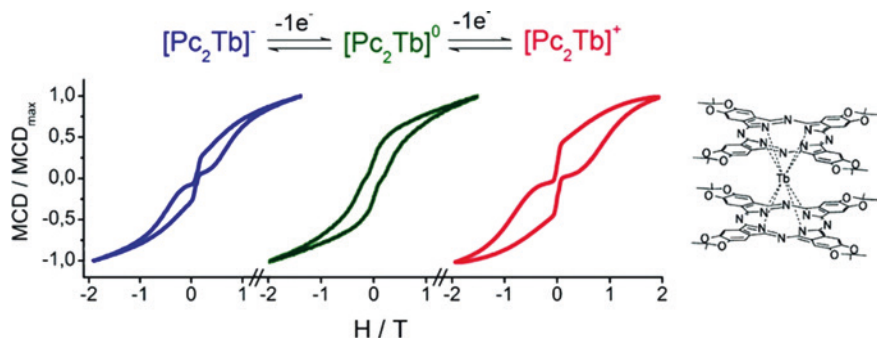


Fig. 2.12 Hysteresis curves of the normalized MCD intensity versus B recorded at 1.5 K and a sweep rate of $1 \text{ T} \cdot \text{min}^{-1}$ for the Q-band of $[\text{TbPc}_2]^-$, $[\text{TbPc}_2]^0$ to $[\text{TbPc}_2]^+$. Reprinted with the permission from Ref. [51]. Copyright 2010 American Chemical Society

the highly reduced states, i.e., the doubly and triply reduced states indicated by the cyclic voltammogram in Fig. 2.13 [53]. The complex contains two substituted Pc ligands, 1,4,8,11,15,18,22,25-octakis-fluoro and 2,3,9,10,16,17,23,24-octakis-perfluoro(isopropyl)phthalocyanine (Pc-CF in Fig. 2.5), where the fluorine-containing groups substitute all peripheral H atoms of Pc ligand, thus stabilizing the highly reduced states due to their strong electron-withdrawing effects. The single-crystal structure for the initial complex, $[\text{Tb}(\text{Pc-CF})_2]\text{-H}$, was obtained by single-crystal X-ray diffraction and shows the clear double-decker sandwiched structure, but one disordered H atom is present over eight nitrogen atoms of the Pc rings to balance the charge. Here, ac magnetic susceptibility measurements were performed for the complex, exhibiting the similar temperature-dependent ac signals to the unsubstituted $[\text{TbPc}_2]$ complex. The barrier was extracted by the Arrhenius fitting to be 365 cm^{-1} at the high-temperature region. Further, the sample solutions of $[\text{Tb}(\text{Pc-CF})_2]^-$, $[\text{Tb}(\text{Pc-CF})_2]^{2-}$, and $[\text{Tb}(\text{Pc-CF})_2]^{3-}$ were prepared by controlled electrolysis at potentials 0.37, -0.03 , and -0.47 V versus SCE, respectively, from the $[\text{Tb}(\text{Pc-CF})_2]\text{-H}$ solution in acetone. The field-dependent MCD spectra recorded at 562, 494, and 705 nm for three samples, respectively, all exhibit the clear hysteresis loops, as seen in Fig. 2.13. Differently, the butterfly-shaped hysteresis was observed in $[\text{Tb}(\text{Pc-CF})_2]^-$ and $[\text{Tb}(\text{Pc-CF})_2]^{3-}$ due to the QTM induced by the hyperfine interactions, while the hysteresis of $[\text{Tb}(\text{Pc-CF})_2]^{2-}$ does not display the narrowing of the loops around zero-dc field. The case is very similar to that occurred in the above $[\text{Ln}(\text{Pc-IPD})_2]^{-/0/+}$ examples. We can draw a key conclusion that the Tb phthalocyanine species with single radical should behave as the better SMMs at zero field due to the suppression of QTM by the coupling interactions between the ground spin ($m_J = \pm 6$) of Tb ion and the ligand spin ($S = 1/2$).

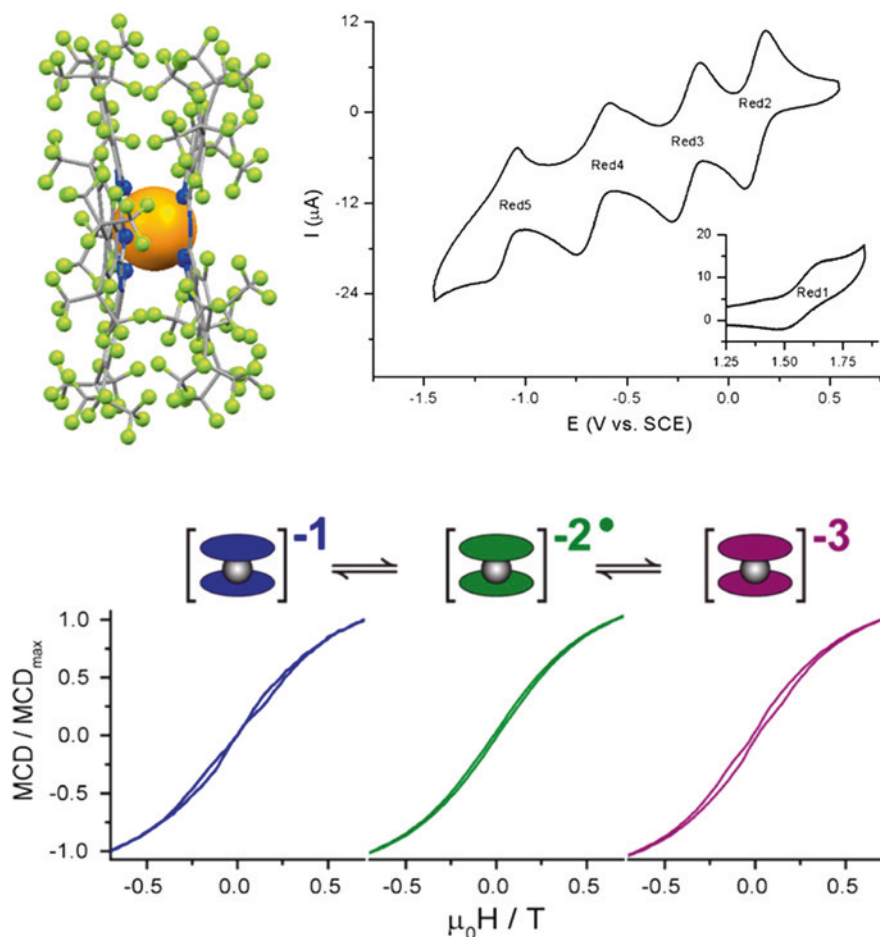


Fig. 2.13 The molecular structure of [Tb(Pc-CF₃)₂]-H, and cyclic voltammogram at 100 mV s⁻¹ of its solution in acetone, as well as hysteresis curves of the normalized MCD intensity recorded at 1.8–1.9 K and at a sweep rate of 1 T min⁻¹. Reprinted with the permission from Ref. [53]. Copyright 2013 American Chemical Society

2.2.4 The Substituted [LnPc₂] SIMMs

To date, a great number of bis(phthalocyaninato) lanthanide double-decker complexes with different substituents at the peripheral positions of the phthalocyanine ring have been synthesized and show the strong SMM behavior, as listed in Table 2.1 [54–59]. In fact, some previous experimental and theoretical investigations have indicated that the electron-donating and electron-withdrawing nature of various substituents have significant effects on the electronic structure, spectroscopic and electrochemistry properties of metal-free phthalocyanines, and, importantly,

Table 2.1 The effective barriers of some typical substituted [LnPc₂] species

Molecule	$U_{\text{eff}}/\text{cm}^{-1}$	τ_0/s	Ref.
[Tb(Pc-OPh) ₂]	504	2.16×10^{-11}	[54]
[Tb(Pc-Oph) ₂] ⁻ N(Me) ₄ ⁺	442	8.2×10^{-11}	[54]
[Tb(Pc-Oph) ₂] ⁻ N(Bu) ₄ ⁺	394	3.45×10^{-10}	[54]
[Tb(Pc)(Pc-Oph)]	652	1.1×10^{-11}	[54]
[Tb(Pc)(Pc-Oph)] ⁻ N(Me) ₄ ⁺	450	3.0×10^{-10}	[54]
[Tb(Pc)(Pc-Oph)] ⁻ N(Bu) ₄ ⁺	487	7.8×10^{-11}	[54]
[Tb(Pc)(Pc-Bu)]	642	2.21×10^{-11}	[54]
[Tb(Pc)(Pc-Bu)] ⁻ N(Bu) ₄ ⁺	400	4.78×10^{-10}	[54]
[Tb(Pc-ODOP) ₂] (order)	480		[55]
[Tb(Pc-ODOP) ₂] (disorder)	422		[55]
[Tb(Pc-a) ₂] ⁻ N(Bu) ₄ ⁺	445	6.35×10^{-11}	[56]
[Tb(Pc-b) ₂] ⁻ N(Bu) ₄ ⁺	428	1.34×10^{-10}	[56]
[Tb(Pc-c) ₂] ⁻ N(Bu) ₄ ⁺	463	2.22×10^{-11}	[56]
[Tb(Pc-OBu) ₂] ₂	230	1.1×10^{-10}	[57]
[Dy(Pc-OBu) ₂] ₂	44	1.3×10^{-5}	[58]
[Dy(Pc-CN) ₂]	40		[59]

further affect the properties of the corresponding coordination complexes with the phthalocyanine ligands. Therefore, such those peripheral modifications for phthalocyanine ligands seem to be critical for finding the SMMs with higher effective barriers.

In 2013, E. Coronado et al. reported a new series of homoleptic and heteroleptic bis(phthalocyaninato) Tb complexes with different peripheral substitution patterns, as seen in Table 2.1 and Fig. 2.14 [54]. The structures of their corresponding neutral radical and anionic forms can be confirmed by the various spectroscopic methods. Here, ¹H NMR spectra were obtained for all complexes and further identified the neutral radical and their reduced forms (Fig. 2.14 top). The magnetic investigations for them demonstrated that all complexes behave as the robust SMMs with the high effective barriers, which were listed in Table 2.1. As a representative example, the neutral heteroleptic [Tb(Pc)(Pc-OPh)] complex shows the well-resolved out-of-phase ac susceptibility maxima that vary with frequency, and the temperature of the χ'' peak at 10,000 Hz reaches up to 58 K, as shown at the bottom of Fig. 2.14. The effective barrier was given according to the Arrhenius formula to be up to 652 cm⁻¹, which represents the highest barrier recorded in the SMM field to date. Several clear trends can be drawn through comparing the magnetic properties of those several complexes. First, all neutral radical complexes exhibit higher barriers than their corresponding anionic complexes, which is consistent with the conclusions in the above section. Second, higher barriers were observed in the heteroleptic phthalocyanine Tb complexes than that in homoleptic complexes. One possible explanation was given by the authors to be that the

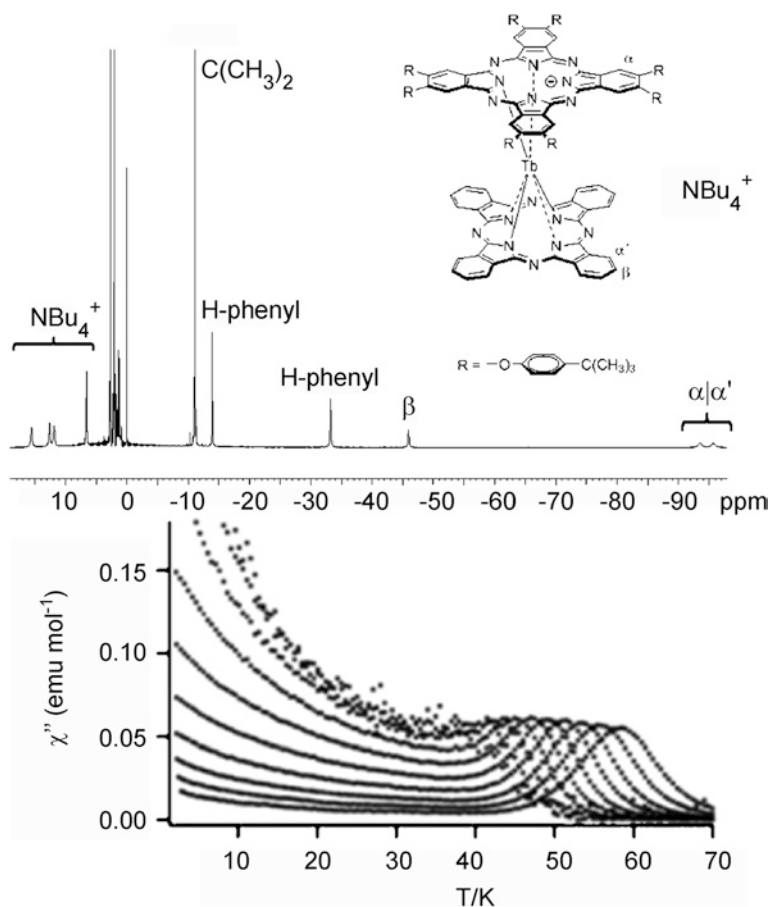


Fig. 2.14 Schematic structure and ^1H NMR spectrum of $[\text{Tb}(\text{Pc})(\text{Pc-Oph})]^- \text{N}(\text{Bu})_4^+$ and ac susceptibility data of its neutral species $[\text{Tb}(\text{Pc})(\text{Pc-Oph})]$ showing the highest effective barrier. Reproduced from Ref. [54] by permission of John Wiley & Sons Ltd.

presence of electron-donating groups on just one of the Pc rings makes the N–Tb distance of the substituted ring larger and, therefore, pushes the metal ion toward the bare Pc ring, thereby enhancing the ligand field of the latter ring [54].

In addition, some other modifications reported have been also presented in Table 2.1, where the very high barriers were demonstrated for the Tb complexes. In particular, the liquid-crystalline terbium double-decker phthalocyanine complex was synthesized in 2010 by using a long chiral alkyl chains to functionalize the $[\text{TbPc}_2]$ core, and further, the complex keeps the strong SMM behaviors of the original core in the disordered and ordered crystalline state [55].

2.2.5 The $[LnPc_2]$ -like SIMMs

Porphyrin, as the structural analogs of phthalocyanine ligand, shows the similar planar tetrapyrrole structure (Fig. 2.5), which thus leads to the assembly of the analogous double-decker structure to the lanthanide ions. The first bis(porphyrinato) double-decker rare earth complex was reported in 1983, but the SMM properties of the Tb complex were firstly explored until recently by Ishikawa and coworkers [60]. Here, the complex can be isolated into two forms, one being the protonated form $[TbH(TPP)_2]$ while the other being the anionic form $[Tb(TPP)_2]^- (H-DBU)^+$ (DBU = 1,8-diazabicyclo[5.4.0] undec-7-ene), which can be determined by the combinations of single-crystal X-ray analysis, NMR, and IR study. For the protonated form, the proton was proved to be located on the nitrogen atom of the TPP pyrrole ring, which thus leads to the different coordination geometry between two forms, as shown in Fig. 2.15. Importantly, the investigations of ac magnetic susceptibilities were indicative of the distinct SMM behaviors for the two forms. Here, no SMM behavior was observed in the protonated form, while the anionic form demonstrated the strongly blocking behavior of magnetization as evidenced by the well-resolved χ'' maxima in Fig. 2.15. Further, the application of a 2000-Oe dc field led to the similar results for them, and the effective barrier can extracted to be 283 cm^{-1} for the anionic complex. This represents a typical example of the double-decker complex whose SMM properties can be reversibly switched by only a single proton.

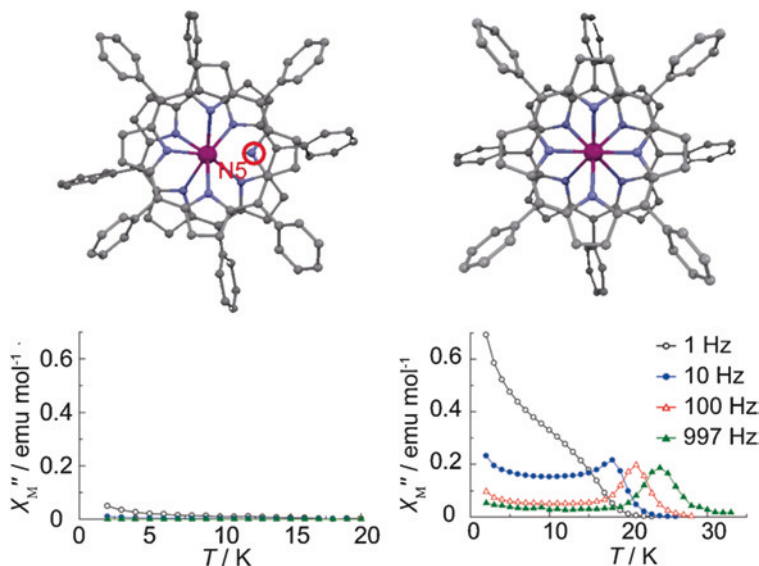


Fig. 2.15 The crystal structure and relaxation dynamics of protonated $[TbH(TPP)_2]$ and deprotonated $[Tb(TPP)_2]^- (H-DBU)^+$. Reproduced from Ref. [60] by permission of The Royal Society of Chemistry

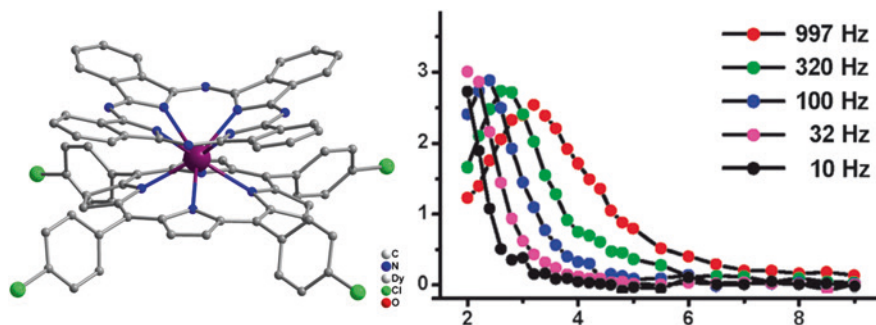


Fig. 2.16 The crystal structure and relaxation dynamics of unprotonated Dy(Pc)(TCIPP). Reproduced from Ref. [61] by permission of The Royal Society of Chemistry

In 2012, J. Jiang et al. reported the magnetic properties of three mixed (phthalocyaninato)(porphyrinato) Dy double-decker complexes, i.e., neutral unprotonated Dy(Pc)(TCIPP) and Dy(Pc-OC5)(TCIPP) and neutral protonated DyH(Pc-OC5)(TCIPP), showing similar sandwich-type double-decker structures to phthalocyanine lanthanide complexes (Fig. 2.16) [61]. A closer look at the crystal structure of three complexes reveals that the complex Dy(Pc)(TCIPP) possesses a SAP geometry with twist angles $\Phi = 43.6^\circ$ closer to the ideal SAP than the other two complexes containing the Pc ligand with non-peripheral substituents. Therefore, obvious temperature-dependent ac signals with χ'' maxima (Fig. 2.16) were observed in the Dy(Pc)(TCIPP) samples, while the other two Dy samples do not show any χ'' peaks under zero-dc field, indicating the presence of slower QTM rates in Dy(Pc)(TCIPP). The magnetic results are well in agreement with the structural changes mainly associated with the twist angle, which provides a typical example to explore correlation between their single-crystal structures and magnetic properties.

In 2012, E.J. Schelter displayed two new double-decker SMMs containing the tetradentate macrocyclic ligands, H₂tmtaa (6,8,15,17-tetramethyl-dibenzotetraaza [14]annulene), which retain the key structural and chemical characteristics of phthalocyanine and porphyrin ligands, as shown in Fig. 2.5 [62]. The double-decker structures were demonstrated in Fig. 2.17. Here, the coordination of tmtaa²⁻ to lanthanide ion leads to a typical saddle conformation, but clearly the double-decker structure is still kept for the two complexes, [Dy(tmtaa)₂K(DME)₂] and [K(DME)(18-crown-6)][Dy(tmtaa)₂]. Nevertheless, the twist angles seem to be so large for the SAP geometry that the geometry is closer to the cube geometry. Therefore, under zero-dc field the fast QTM relaxation is present in both two undiluted complexes, as indicated by the increasing χ'' signals with the decreasing of temperature, which is as a result of the increased transversal anisotropy from the decreased symmetry for the coordination geometry around Dy ion. Further, the combinations of the magnetic dilution in the isostructural Y complexes and the application of a 100-Oe dc field lead to the occurrence of the thermally activated relaxation in a wider temperature range, as seen in Fig. 2.17. The barriers were able to be extracted to be 28.4 and 34.6 K, respectively, for two diluted samples.

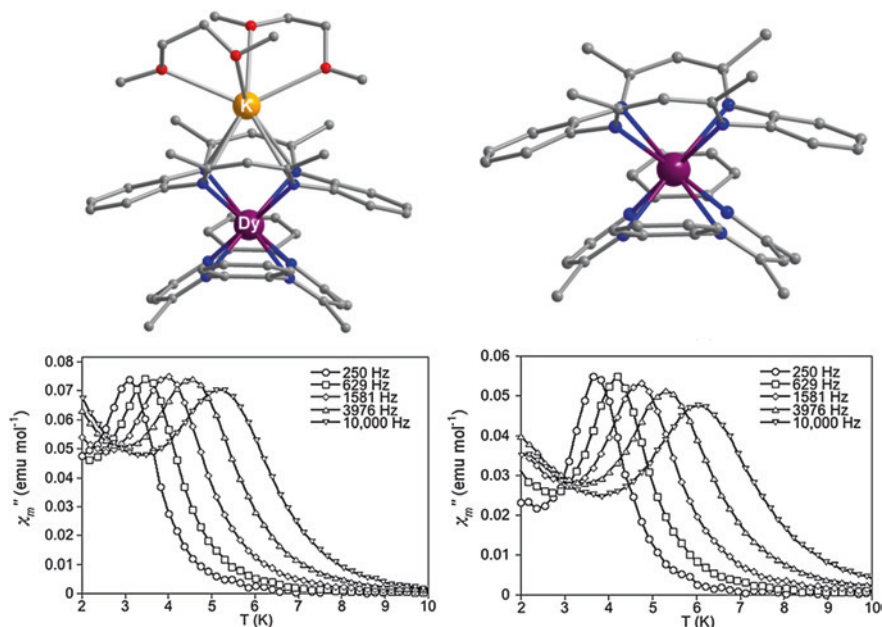


Fig. 2.17 The crystal structure and relaxation dynamics of $[\text{Dy}(\text{tmtaa})_2\text{K}(\text{DME})_2]$ and $[\text{K}(\text{DME})(18\text{-crown-6})][\text{Dy}(\text{tmtaa})_2]$. Reproduced from Ref. [62] by permission of The Royal Society of Chemistry

Consequently, the magnetic exploration into the porphyrin and other double-decker lanthanide complexes further expend the field of phthalocyanine lanthanide SIMMs and open the door to new experiments, potentially allowing the discovery of lanthanide SIMMs with higher effective barriers.

2.2.6 The *LnPOM* SIMMs

Polyoxometalates (POM) are built from the connection of $[\text{MO}_x]$ polyhedrons with M being a *d*-block element in high oxidation state, usually $\text{V}^{\text{IV,V}}$, Mo^{VI} , or W^{VI} [39]. In the past few years, the POM-based complexes have been investigated extensively for use in various applications from catalysis, medicine, electrochemistry, photochromism, to magnetism. The lanthanide POM complex (*LnPOM*) was firstly investigated to show the SMM behavior in 2008 [12] and they are seen as the second lanthanide SIMM family discovered following the $[\text{LnPc}_2]$ SIMMs. Figure 2.18 shows the structure features of *LnPOM* and the electronic levels of lanthanide ions under the crystal field constructed from the POM ligands [63]. The coordination geometry around lanthanide ions, at a first glance, is very similar to the SAP geometry of phthalocyanine lanthanide complexes with the twist angle of

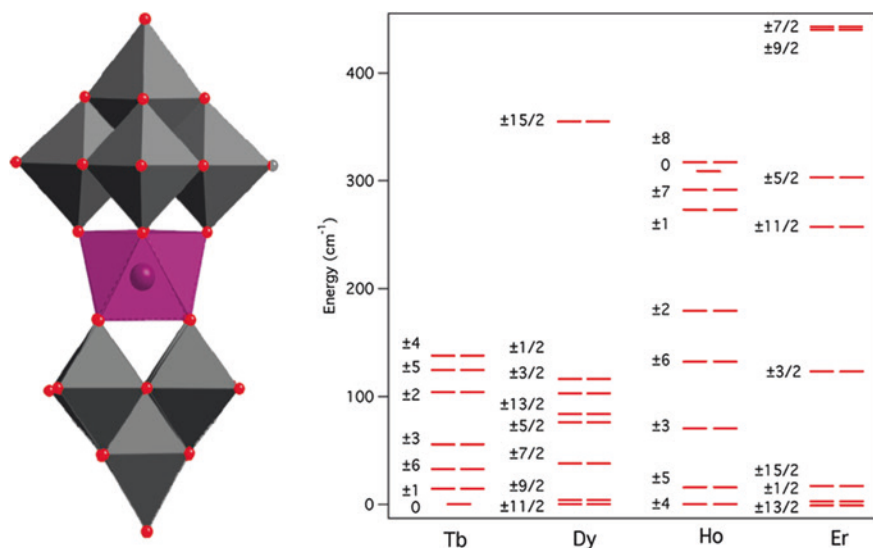


Fig. 2.18 The structure features of LnPOM and the electronic levels of lanthanide ions under the crystal field constructed from the POM ligands. Reprinted with the permission from Ref. [63]. Copyright 2009 American Chemical Society

44.2°, but a detailed analysis for their structures reveals a certain axial compression of the SAP geometry around lanthanide ions indicated by $d_{pp} < d_{in}$, which is opposite to that of the phthalocyanine lanthanide complexes. As predicted by the calculations in Sect. 2.1, these geometrical differences in the crystal fields, although small, seem to be sufficient to completely change the electronic structures of lanthanide ions as shown in Fig. 2.18. Contrary to the phthalocyanine lanthanide complexes (Fig. 2.8), the Tb, Dy, and Ho complexes show the ground state with the relatively small m_J value, while a large spin ground state $m_J = \pm 13/2$ is discovered in ErPOM. Therefore, the distinct electronic structures from [LnPc₂] complexes result in the different relaxation dynamics for them.

As indicated by the electronic levels diagram (Fig. 2.18), the ErPOM behaves as the best SMM in the series of lanthanide complexes. Ac magnetic susceptibility measurements show the typical features associated with the SMM behavior, i.e., the temperature-dependent peaks of the out-of-phase component of the ac susceptibility between 1000 and 10,000 Hz (Fig. 2.19). The effective barrier was given to be 55.2 K by the linear fitting of $\ln \tau$ versus $1/T$. For Tb, Dy, and Ho ions, only Ho complex shows the weak χ'' signal with a shoulder, indicating the fast competing QTM relaxation.

In addition, a new LnPOM family showing the unusual C_5 axial symmetry was explored in magnetism by Coronado et al. [64]. Here, the Dy and Ho derivatives show the weak slow relaxation of magnetization, which will not be introduced in detail.

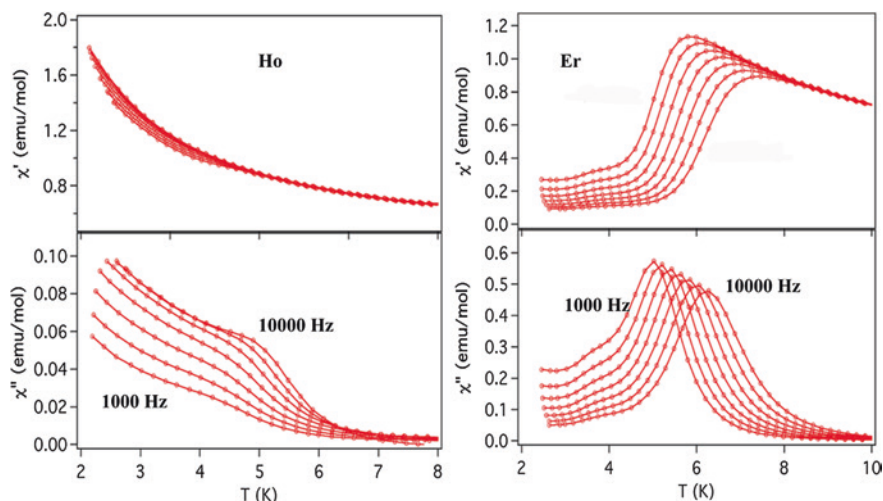


Fig. 2.19 The temperature-dependent out-of-phase component of the ac susceptibility signals between 1000 and 10,000 Hz for HoPOM and ErPOM. Reprinted with the permission from Ref. [63]. Copyright 2009 American Chemical Society

Up to now, the $[\text{LnPc}_2]$ and LnPOM SIMMs have been reviewed from a viewpoint of achieving the high-performance SMMs for the envisaged technological applications of these molecules as classical or quantum bits. It is well known that the two species, especially the $[\text{LnPc}_2]$, play an outstanding role in the development of SMM, because they open the door to lanthanide SMM field and the good performances stimulate the successful development of other following SMMs.

2.3 Lanthanide β -diketone Systems

A β -diketone behaves as a monobasic acid in solutions or solids, as the keto-enol tautomerisms easily lead to the deprotonated form in an appropriate pH range, as seen in Fig. 2.20. Thus, the β -diketone can act as a mononegative bidentate ligand to coordinate to a lanthanide ion and forms stable lanthanide complexes. In fact, such complexes have been widely investigated in some other fields, especially for the photoluminescence, where β -diketones have been recognized as efficient sensitizers to achieving high-harvest lanthanide emissions [40]. In the field of molecular magnetism, the magnetic study for them should start with the lanthanide complexes containing radical ligands [6, 65], whose synthesis almost begin with the reactions between the fluorinated β -diketones lanthanide complexes and the corresponding radicals due to the high solubility of fluorinated β -diketones lanthanide complexes in organic solvents. However, the real development in magnetism for this kinds of complexes should date back to 2010, when S. Gao et al.

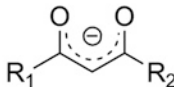
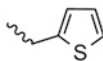
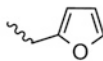
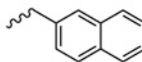
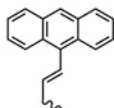
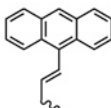
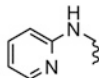
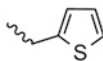
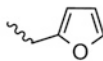
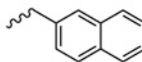
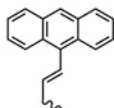
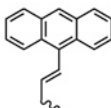
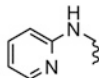
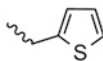
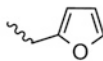
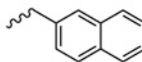
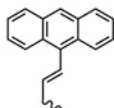
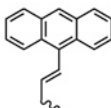
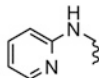
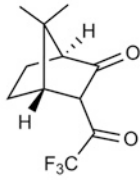
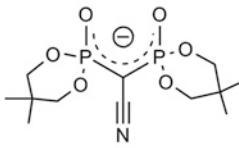
 <p>L1</p>	<table><tr><th>R₁</th><th>R₂</th><th>abbreviation</th></tr><tr><td>—CH₃</td><td>—CH₃</td><td>acac</td></tr><tr><td>—CH₃</td><td>—CH₂CH₃</td><td>acec</td></tr><tr><td>—CF₃</td><td>—CF₃</td><td>hfac</td></tr><tr><td>Ph</td><td>Ph</td><td>Phacac</td></tr><tr><td>Ph</td><td>—CF₃</td><td>tfnb</td></tr><tr><td></td><td>—CF₃</td><td>tta</td></tr><tr><td></td><td>—CF₃</td><td>fta</td></tr><tr><td></td><td>—CF₃</td><td>nta</td></tr><tr><td></td><td></td><td>accm</td></tr><tr><td></td><td>—CH₃</td><td>paaH</td></tr></table>	R ₁	R ₂	abbreviation	—CH ₃	—CH ₃	acac	—CH ₃	—CH ₂ CH ₃	acec	—CF ₃	—CF ₃	hfac	Ph	Ph	Phacac	Ph	—CF ₃	tfnb		—CF ₃	tta		—CF ₃	fta		—CF ₃	nta			accm		—CH ₃	paaH
R ₁	R ₂	abbreviation																																
—CH ₃	—CH ₃	acac																																
—CH ₃	—CH ₂ CH ₃	acec																																
—CF ₃	—CF ₃	hfac																																
Ph	Ph	Phacac																																
Ph	—CF ₃	tfnb																																
	—CF ₃	tta																																
	—CF ₃	fta																																
	—CF ₃	nta																																
		accm																																
	—CH ₃	paaH																																
 <p>L2</p>																																		
 <p>L3</p>																																		

Fig. 2.20 β -diketone ligands with different substituent groups used in lanthanide SMMs

reported the tri(β -diketones) Dy complex, $[\text{Dy}(\text{acac})_3(\text{H}_2\text{O})_2]$, functioning as the efficient SMM [8]. Here, three β -diketone ligands and two coordinating H_2O molecules form the eight coordinate quasi-SAP geometry close to the D_{4d} symmetry. Therefore, the authors attributed the SMM behavior to the high symmetry of this complex similar to the $[\text{LnPc}_2]$ SMMs, and the CONDON calculations were performed based on the local D_{4d} symmetry, indicating the ground doublets with an Ising-type axial anisotropy. Such an idea further stimulated a series of magnetic investigations for this kind of β -diketone lanthanide complexes in expectation of obtaining the high-barrier SMMs [13]. In fact, some groundbreaking results have been achieved, which mainly benefit from the stable structures of this kind of complexes. It is noteworthy that the two H_2O molecules in seminal complex are easily substituted by other auxiliary ligands, especially the bidentate capping ligands as shown in Fig. 2.21, and thus, modifications can be easily incorporated into the coordination geometry in the β -diketone-based complexes. In addition, as

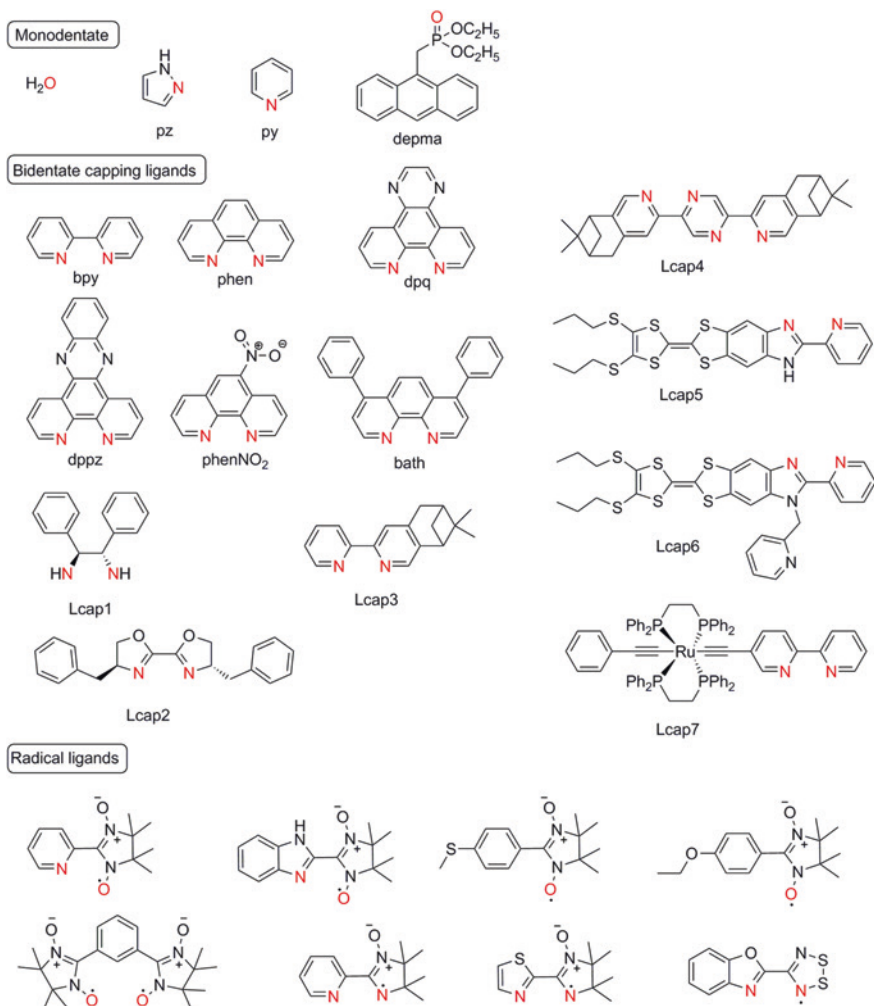


Fig. 2.21 Auxiliary ligands used in lanthanide β -diketone systems

shown in Fig. 2.20, it is variety for β -diketone ligands showing the different substituents at the R_1 and R_2 positions, which thus provides the advantage of systematically exploring the factors governing their magnetic properties.

2.3.1 The Magnetism of $[\text{Dy}(\text{acac})_3(\text{H}_2\text{O})_2]$

The structure has been described above as the quasi- D_{4d} symmetry in the first coordination sphere, which seems to be highly uniaxial symmetric, leading to the obvious slow relaxation of magnetization [8]. However, as seen in

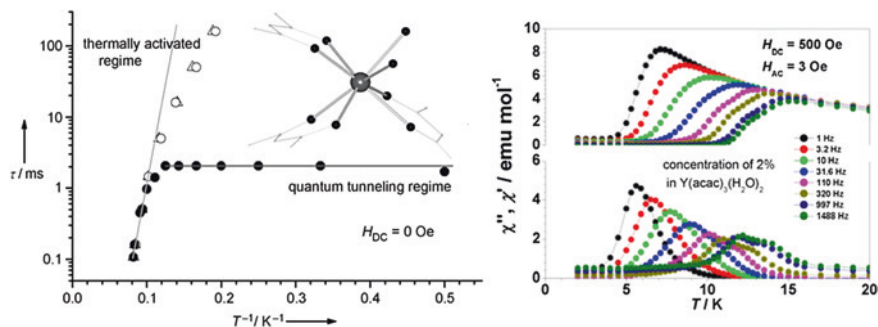


Fig. 2.22 *Left* The relaxation time (τ) of $[\text{Dy}(\text{acac})_3(\text{H}_2\text{O})_2]$ at different concentrations in $[\text{Y}(\text{acac})_3(\text{H}_2\text{O})_2]$ in the temperature range 2–12 K (filled marks undiluted samples; open marks diluted samples). *Right* The temperature dependence of the ac susceptibility from 1 to 1488 Hz for the 50 times diluted Dy by Y complex at a dc field of 500 Oe. Reproduced from Ref. [8] by permission of John Wiley & Sons Ltd.

Fig. 2.22, the temperature-independent region in the $\ln(\tau)$ versus $1/T$ plots is indicative of the presence of fast QTM relaxation pathway at low temperature, which should arise from some asymmetric factors in the local molecule or the relatively short intermolecular distances. To further get insight of the magnetic behavior and reduce QTM relaxation, magnetic dilutions were performed. The results show that the enhanced SMM behavior was observed, but an increasing χ'' signal with the decreasing temperature is still indicative of the occurrence of QTM at low temperature, i.e., the spin moments cannot be blocked completely. Further, the combination of magnetic dilution and the application of a dc field resulted in the perfect suppression of QTM relaxation, as evidenced by the nearly vanishing χ'' signals at low temperature in Fig. 2.22. The effective barrier was able to be fitted by the Arrhenius law to be 44.7 cm^{-1} (64 K). Here although the barrier seems to be not so high when compared to that of $[\text{TbPc}_2]$ complexes, the detailed investigations for magnetic properties of the complex initiated a new SIMM family after the $[\text{LnPc}_2]$ and LnPOM SIMMs.

2.3.2 The Modulations of Auxiliary Ligands

A successful modulation of SMM properties for the seminal complex was performed by J. Tang and coworkers [13]. Here, the two H_2O molecules in the seminal complex are replaced by 1,10-phenanthroline (phen) and its large aromatic derivatives (dpq and dppz in Fig. 2.21), which leads to the constructions of three new SIMMs keeping the nearly D_{4d} local symmetry of the similar complex. Here, the complex, $[\text{Dy}(\text{acac})_3(\text{phen})]$, displays the similar SMM properties with the almost same barrier to that of the seminal complex. Nevertheless, it is worth

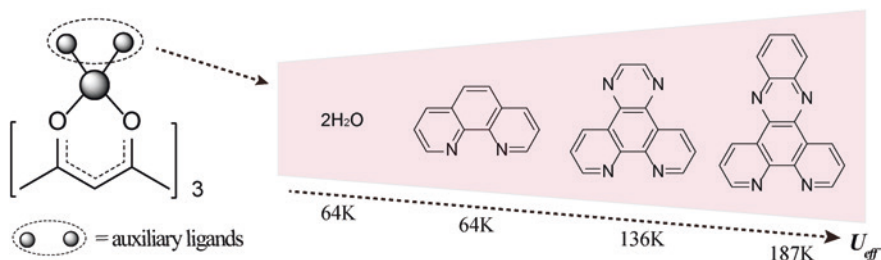


Fig. 2.23 Schematic structures and effective barriers of the Dy β -diketone complexes with different auxiliary ligands

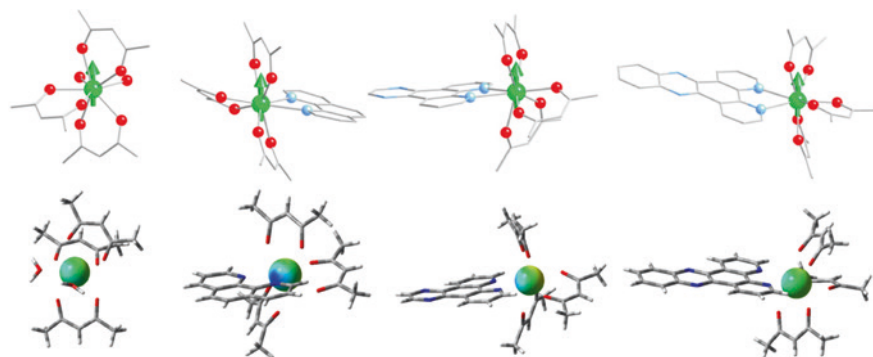


Fig. 2.24 *Top* The anisotropic axes of four Dy β -diketone complexes with auxiliary ligands H_2O , phen, dpq, and dppz. *Bottom* Their electrostatic potential originated from the ligand environment mapped into a sphere centered in the position of the Dy cation with radius 1.0 Å. The color scale between more (red) and less (blue) negative potential is always 0.065 a.u. Reprinted with the permission from Ref. [66]. Copyright 2013 American Chemical Society

noting that two another complexes with larger aromatic groups show the very high barriers, 136 and 187 K, which are two and three times larger than that of the seminal complex, as seen in Fig. 2.23.

A possible reason for their SMM behaviors was given as the strong uniaxial anisotropy arising from the nearly D_{4d} local symmetry, but it is difficult to explain the greatly increasing of effective barriers by replacing the auxiliary ligands. Significantly, the recent *ab initio* and electrostatic potential models calculations from E. Ruiz indicated that the anisotropy axis is not parallel to the quasi- S_8 axis of the local coordination geometry around Dy ion, but passes through the two trans- β -diketonate ligands for those complexes, as shown in Fig. 2.24 [66]. Therefore, it is more reasonable to explain the strong SMM behaviors through the electrostatic potential models for the series of lanthanide complexes. Here, the Dy ion is located in the plane constructed by the delocalized negative charge in two trans- β -diketonate ligands, leading to the strong repulsing interactions. Based on the rules of the electrostatic energy minimization, the radial plane of the oblate electron

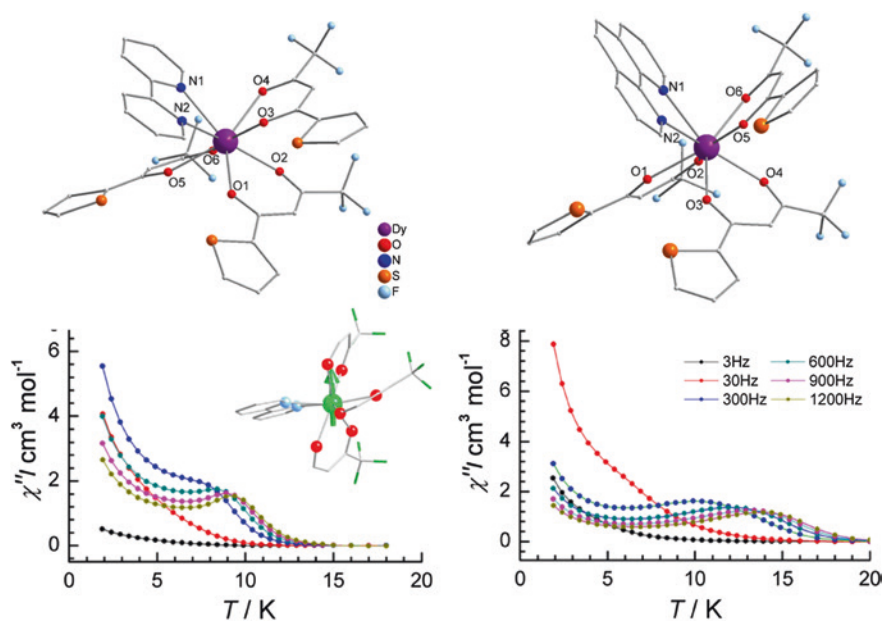


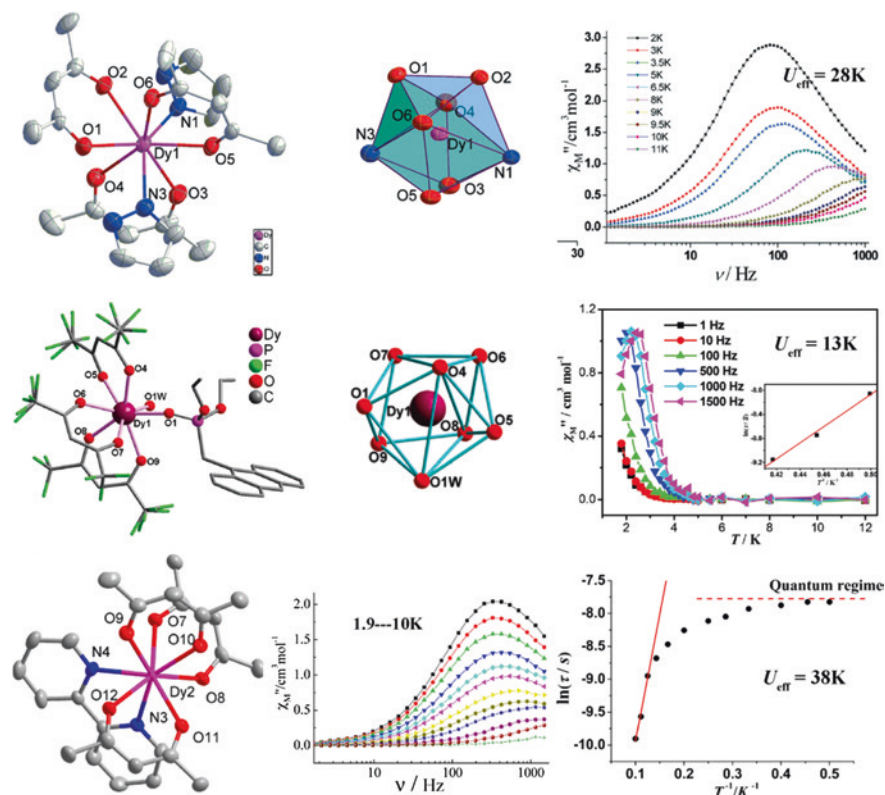
Fig. 2.25 The crystal structures and relaxation dynamics of Dy- β -diketones systems with tta and bpy/phen ligands. Reproduced from Ref. [68] by permission of John Wiley & Sons Ltd. *Inset*, Reprinted with the permission from Ref. [66]. Copyright 2013 American Chemical Society

density of Dy ion is thus coincident with the plane with only one charged ligand, and the anisotropy axis is parallel to the plane with two trans- β -diketonate ligands [67]. Electrostatic potential maps calculated for all four complexes show a similar electrostatic potential shape with a small less negative region originated by the neutral ligands and a more repulsive environment closer to the negative ligands, as shown in Fig. 2.24 [66]. Considering the above explanation for the magnetic anisotropy, we could deduce that the large delocalized effect in the neutral ligands may have a pronounced effect on reducing the repulsive interactions of their coordinate atoms at the plane perpendicular to the anisotropy axis, which, relatively, enhance the axial crystal effects. Consequently, it is possible to explain the increasing effective barriers by substituting the small ligands to the large aromatic derivatives with delocalized π -electrons. Nevertheless, it should note that the magnetic properties are extremely sensitive to small changes in the structure of the complexes, as shown by the experimental and theoretical study of the strong influence on magnetic anisotropic properties of the rotation of the hydrogen atoms in the water ligands in mononuclear Dy^{III} complexes [24], so further experimental and theoretical study should be performed for the better understanding of their magnetic properties.

Another Dy- β -diketone system with tta (tta = 4,4,4-trifluoro-1-(2-thienyl)-1,3-butanedionate) and bpy/phen has also been developed by our group with the goal of identifying features relevant to modulating relaxation dynamics of single-ion magnets, as shown in Fig. 2.25 [68]. Similarly, the O₆N₂ environment forms an

approximately SAP coordination polyhedron, with the similar α angles of 57.2 and 56.4° and remarkable difference in the skew angle of 39.7 and 42.1° for two complexes, respectively. The structures are still described as SAP geometry and the anisotropy axis also passes through the two trans- β -diketonate ligands (Fig. 2.25 inset) [66], consistent with that of the above examples. Their ac magnetic susceptibility signals were shown in Fig. 2.25, both showing the increasing out-of-phase χ'' signals with a shoulder indicative of the fast QTM at low temperature. At the linear regimes of $\ln(\tau)$ versus $1/T$ plots, the effective barriers were extracted to be 58 and 85 K, which are of the same order of magnitude as that of the seminal complex, for two complexes with bpy and phen ligands, respectively. The small increase in effective barriers for $[\text{Dy}(\text{tta})_3(\text{phen})]$ than $[\text{Dy}(\text{tta})_3(\text{bpy})]$ may be as a result of the stronger delocalized effects in the phen ligand than in the bpy ligand.

In addition, several typical Dy-based SIMMs based on hexafluoroacetylacetonate (hfac) were reported by the different research groups, as shown in Fig. 2.26 [69–71]. Compared with the seminal complex, for the first two complexes the



H_2O was substituted by the larger monodentate ligands, leading to the low-symmetry coordination geometry around Dy ions, while the bidentate bpy ligand was applied to replace two H_2O in the third complexes and thus the complex keeps the quasi- D_{4d} geometry. Nevertheless, no obvious changes in SMM properties were observed for the three complexes, and their SMM properties were weakened in contrast to that of the seminal complex, as indicated by their small effective barriers labeled in Fig. 2.26. The reduced SMM behavior may be due to the lowered symmetry around Dy ions and the strong electron-withdrawing effects of fluorine atoms, which may greatly reduce the strength of the axial crystal field. Finally, it is worth noting that this kind of fluorinated β -diketones lanthanide complexes shows the enhanced luminescence behavior with reducing the acidity of the β -diketones compared with the conventional β -diketone ligands, which thus provide a promising approach to design multifunctional lanthanide SMMs.

To date, all the β -diketones lanthanide SIMMs discussed above are Dy-based complexes, which mainly depends on the electronic structures of Dy ions and its Kramers ion properties. In contrast, for another Kramers ion Er^{3+} with the distinct electronic structures from Dy ion, the magnetism of a series of β -diketones complexes was also explored recently by Silva [72], as shown in Fig. 2.27. Here, 2,4-hexanedione (acac) ligands and three bidentate capping ligands were applied to construct three complexes with the typical

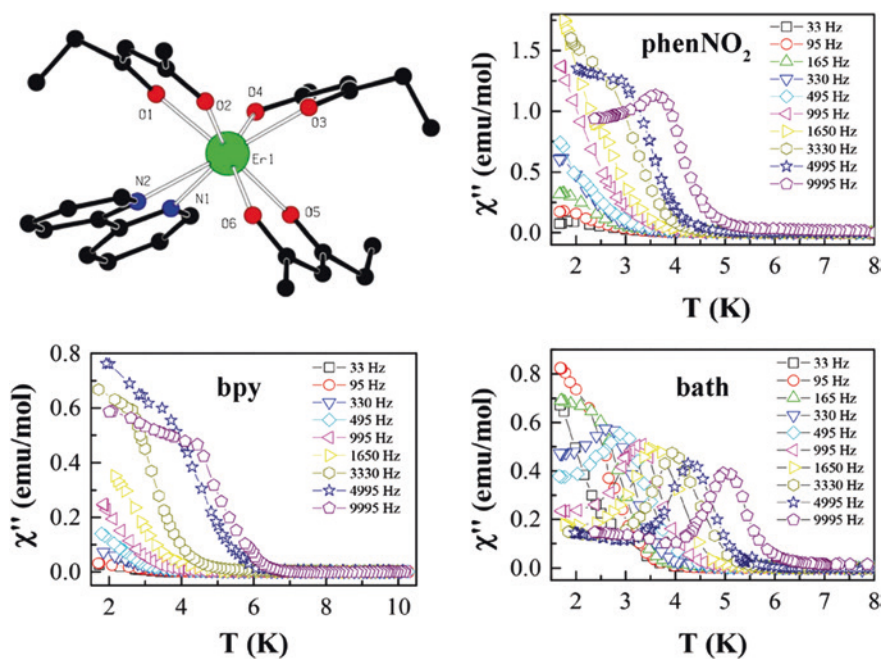


Fig. 2.27 The Er-based β -diketone systems with acac ligands and three different bidentate capping ligands. Reproduced from Ref. [72] by permission of The Royal Society of Chemistry

coordination geometry, $[\text{Er}(\text{acec})_3(\text{Lcap})]$ ($\text{Lcap} = \text{bpy}$, phenNO_2 and bath in Fig. 2.21). All three complexes display the typical field-induced slow relaxation of magnetization under a 1000-Oe dc field, as evidenced by the obvious χ'' signals shown in Fig. 2.27. In contrast to the other two complexes, the third complex with bath ligand behaves as the best SMM by introducing the larger auxiliary ligands. Nevertheless, the effective barriers for three complexes are still very low, only 8, 13, and 23 K, respectively, and thus the further modifications are necessary.

2.3.3 Chiral β -diketone Dy SIMMs

Due to the stable structures as seen above, some additional functions can be easily incorporated into the β -diketone lanthanide systems by the modifications of the auxiliary ligands or β -diketone ligands, while maintaining their typical structural features and the robust SMM behavior. The most typical examples are the design and assembly of chiral SMMs showing certain physical properties such as ferroelectricity, piezoelectricity, second harmonic generation (SHG), and magneto-chiral dichroism (MChD) effects [73], and to date several complexes have been reported containing the auxiliary ligands from Lcap1 to Lcap4 in Fig. 2.21 [73–77]. Here, only two typical examples were discussed below to present the useful synthetic approach of chiral SMMs for readers.

Figure 2.28 shows the crystal structures of the enantiomeric pair of Dy β -diketone complexes (R -1 and S -1), where the chirality is clearly introduced by transferring chiral information of auxiliary ligands (Lcap4 in Fig. 2.21) to the paramagnetic assemblies [73]. The two complexes crystallized in chiral space groups $P2_12_12_1$ and the solid-state CD spectra confirmed their chiroptical activity and enantiomeric nature. Here, the changes of β -diketone and auxiliary ligands lead to the bicapped trigonal prism geometry around Dy ions, diverging from the SAP geometry of the seminal complex. Even so obvious SMM behaviors were still observed below 20 K at zero-dc field for them, which was shown in Fig. 2.28. The effective barrier was extracted by Arrhenius law to be 47 K, slightly smaller than that of the seminal complex.

In addition, two enantiomeric pairs of β -diketone Dy SIMs were assembled in 2013 using a pair of homochiral β -diketonate ligands L2 in Fig. 2.20 [77]. It is worth noting that their SMM behaviors can be modified through changing the auxiliary ligands (bpy and phen in Fig. 2.21), as shown in Figs. 2.29 and 2.30. Similarly, both two complexes crystallized in chiral space groups and the solid-state CD spectra also confirmed their chiroptical activity and enantiomeric nature. For the complexes with bipyridine ligands, two types of homochiral stereoisomers are cocrystallized together in the crystal structure, as shown in Fig. 2.29. Here although two stereoisomers demonstrate the same molecular formula, the distinct structures are observed for them displaying the different distorted SAP geometries. The ac magnetic susceptibilities measurements display the weak ac signals with no peaks under zero-dc field,

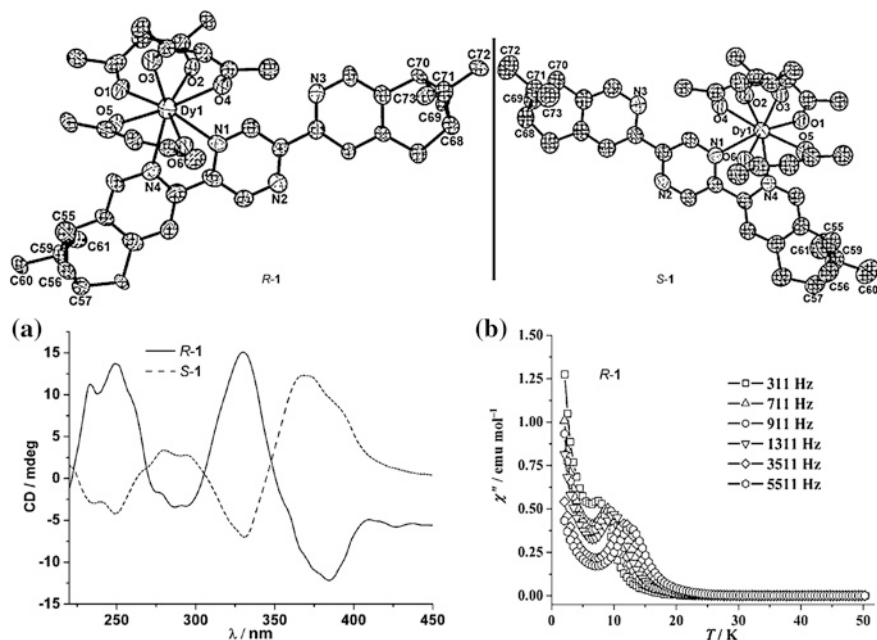


Fig. 2.28 The crystal structures, CD spectra, and relaxation dynamics of the enantiomeric pair of Dy β -diketone complexes with chiral auxiliary ligands Lcap4. Reproduced from Ref. [73] by permission of John Wiley & Sons Ltd.

indicating the onset of slow relaxation of magnetization. Further, the application of a 1000-Oe dc field leads to the occurrence of two thermally activated relaxation processes revealed by the presence of two distinct peaks for the out-of-phase ac signals in Fig. 2.29, which may be related to the presence of two crystallographically independent Dy^{III} centers in crystal structure. The effective barriers were given to be 36.5 and 46 K, respectively.

The complexes with phen ligands in Fig. 2.30 also adopt a distorted SAP coordination geometry with the phen capping ligand instead of the bpy capping ligand of the above complexes. Here, the SMM behavior was not observed under a zero-dc field, but the application of a 1000-Oe dc field leads to the occurrence of single relaxation process, as shown in Fig. 2.30. The effective barrier was given to be 30.5 K with $\tau_0 = 1.1 \times 10^{-7}$ s.

2.3.4 The SIMMs with Large Capping Ligands

In recent years, the synthesis and coordination chemistry of electro-active molecules functionalized by various mono- or polydentate groups have developed to be the focus of much attention. For example, the tetrathiafulvalene (TTF) derivatives

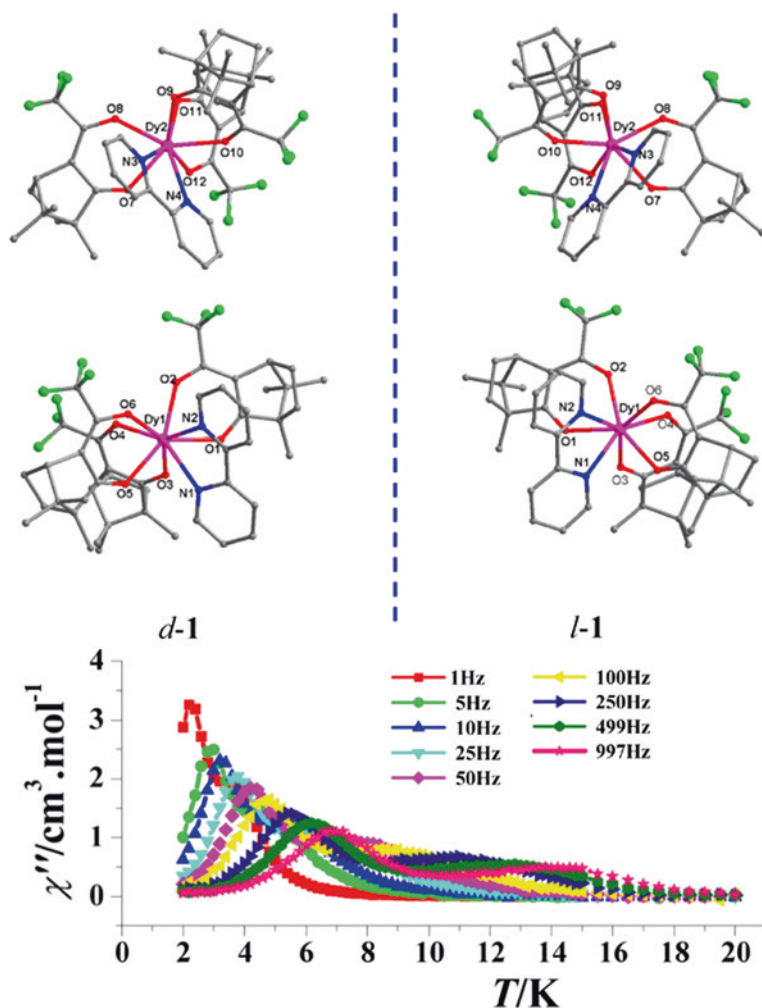


Fig. 2.29 The crystal structures, and relaxation dynamics of the enantiomeric pair of Dy β -diketone complexes with chiral β -diketone ligands L2 and auxiliary ligand bpy. Reprinted with the permission from Ref. [77]. Copyright 2013 American Chemical Society

with the delocalized π electrons showing the strong redox-active properties have been extensively studied in molecular conductors and superconductors [78, 79]. In particular, the redox-active TTF molecules coordinating heteroatom-based groups can be directly coupled with the localized unpaired electrons, which lead to the so-called π - d systems consisting of the delocalized π and localized d electrons, displaying some novel transport properties [80]. In addition, group 8 metal acetylide complexes displaying strong ligand-mediated electronic effects are attractive redox-switchable building blocks for the realization of optical or conductive

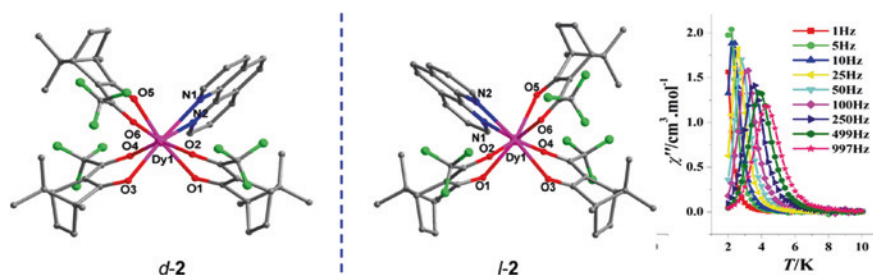


Fig. 2.30 The crystal structures and relaxation dynamics of the enantiomeric pair of Dy β -diketone complexes with chiral β -diketone ligands L2 and auxiliary ligand phen. Reprinted with the permission from Ref. [77]. Copyright 2013 American Chemical Society

switches [81, 82]. Therefore, the above materials provide the great potential applications in multifunctional materials combining the light, electronic, and magnetic properties. However, this kind of ligands is rarely explored in the synthesis of lanthanide SIMMs to date. Here, those ligands containing bipyridine-type ligands (Lcap5–Lcap7 in Fig. 2.21) are very suitable for the auxiliary ligands of the β -diketone Dy complexes, which provide a great platform for studying this kind of lanthanide SIMMs.

In 2012, the β -diketone Dy SIMM functionalized by a ruthenium carbon-rich moiety (Lcap7 in Fig. 2.21) was presented by Norel et al. [83]. The structure was shown in Fig. 2.31, where the classical SAP geometry is still kept around Dy ion in spite of the large volume of auxiliary ligands. The ac magnetic susceptibilities measurements at zero-dc field display the temperature-dependent χ'' maxima at the high-temperature region and a temperature-independent quantum tunneling region. Notably, as shown in Fig. 2.31b, the application of a dc field results in the occurrence of multiple relaxation processes, which is not observed in the conventional β -diketone examples. It is an important issue to be discussed for the reasons of the multiple relaxation processes, which may be related to the strong ligand-mediated electronic effects. Clearly, the external dc field of 480 and 1000 Oe can significantly reduce the efficiency of the underbarrier process, as indicated by the slowing quantum tunneling relaxation times (Fig. 2.31). Under the dc field of 1000 Oe, two effective barriers were extracted to be 11 and 33 K at the low- and high-temperature regions, respectively.

In 2013, E. Pointillart et al. reported the magnetic investigations of two mononuclear β -diketone Dy complexes which were built from the reaction of the auxiliary ligands Lcap5/Lcap6 and $\text{Dy}(\text{hfac})_3 \cdot 2\text{H}_2\text{O}$ [32]. Here, the strong π – π interactions and hydrogen bonds in the crystal structure lead to the formation of head-to-tail dimers. For the complex $[\text{Dy}(\text{hfac})_3(\text{Lcap5})]$, no any out-of-phase signals in zero-dc field were observed, while complex $[\text{Dy}(\text{hfac})_3(\text{Lcap6})]$ shows a clear out-of-phase ac signal below 8 K in zero-dc field. In particular, the diluted samples of $[\text{Dy}(\text{hfac})_3(\text{Lcap6})]$ demonstrate a quantum tunneling time nearly 30 times slower than in the pure compound. In addition, the multiple relaxation processes were

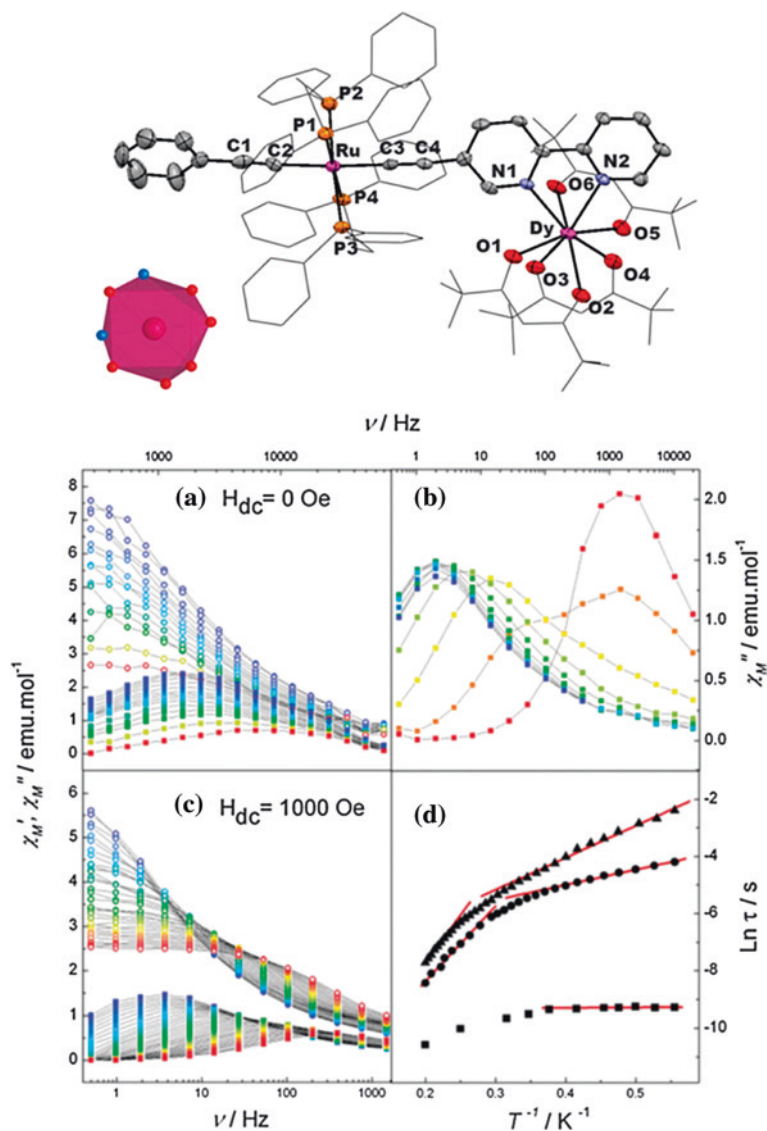


Fig. 2.31 The crystal structure and ac susceptibility data of Dy β -diketone system with capping ligand Lcap7 containing a ruthenium carbon-rich moiety. Reproduced from Ref. [83] by permission of The Royal Society of Chemistry

also observed through the application of an appropriate dc field. Further, the substitution of β -diketone ligand hfac by tta ligand leads to the formation of complex $[\text{Dy}(\text{tta})_3(\text{Lcap6})]$, whose magnetic properties were investigated systematically by angular-resolved magnetometry and MCD measurement and ab initio calculations, as seen in Fig. 2.32. Here, the angular-resolved magnetometry measurement indicated

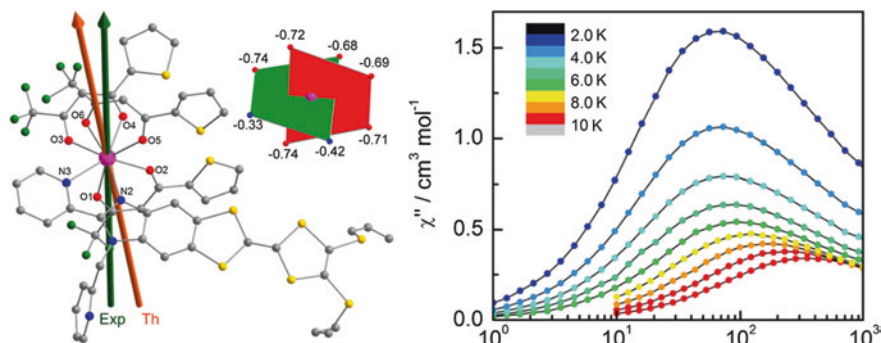


Fig. 2.32 The crystal structure, magnetic anisotropic axis and relaxation dynamics of [Dy(hfac)₃(Lcap6)]. Reprinted with the permission from Ref. [32]. Copyright 2013 American Chemical Society

that the strong Ising-type anisotropy axis is almost parallel to the red plane in Fig. 2.32 and passes through the two trans- β -diketonate ligands, which is consistent with the results of ab initio calculations with only a small deviation of 7.6°. The complex shows the similar relaxation dynamics properties to [Dy(hfac)₃(Lcap6)] under zero- or nonzero-dc field with only a small increase of effective barriers. Notably, the hysteresis loops at 2 K can be recorded in the MCD spectrum on a solid solution, highlighting the molecular origin of magnetization dynamics.

2.3.5 The SIMMs with Radical Ligands

To date, the most widely investigated family of radical ligands in the field of lanthanide molecular magnets is the nitronyl nitroxide radical systems (NIT-R in Fig. 2.21), which show the high stability and the strong coordinate ability to lanthanide ions in the β -diketone lanthanide systems [84]. Nowadays, a great number of such lanthanide complexes have been reported, ranging from the mononuclear, binuclear and even to single-chain complexes bridged by the NIT radicals. As is well known, the first rare earth-radical-based coordination polymer exhibiting SCM behavior was reported in 2005 by Sessoli [65]. In the chain molecule, the radical NIT-C₆H₄OPh plays an important bridging role between the Dy ions, leading to a low ratio of interchain/intrachain interactions. In addition, several binuclear Tb complexes bridged by the NIT-R radical ligands show the strong SMM behavior, which will be discussed in next chapter. In contrast, the reported mononuclear Tb/Dy complexes with the NIT-R radical demonstrated the relatively weak SMM behavior and fast QTM [85–93]. Here, only two representative examples were exhibited. In addition, other types of radical systems were also explored recently with some examples showing the strong SMM behavior, which further expand this field in pursuit of the better lanthanide–radical SMM systems.

As shown in Fig. 2.33, the monodentate and bidentate chelate NIT-R radical ligands lead to the distinct structures in lanthanide coordination complexes due to their different coordinate modes. In the first example, $[\text{Tb}(\text{hfac})_3(\text{NIT-PhOEt})_2]$, two radical ligands are coordinating to the central Tb ion through the oxygen atom of one N-O group, leading to the novel mononuclear tri-spin lanthanide system, where the Tb ion is located in a distorted dodecahedron geometry [85]. The continuously increasing $\chi_m T$ values with the decreasing temperature are indicative of the strong ferromagnetic interactions between Tb ion and the radical ligands. Importantly, the clear blocking behavior of magnetization was observed in the complex, as indicated in the ac susceptibility signal under zero-dc applied field in Fig. 2.33. The effective barrier was given to be 29 K, which seems to be so small compared to the above lanthanide SMM. For the second example, the bidentate radical ligand provides a same coordinate mode to the common capping ligand, thus leading to the formation of the similar coordinate geometry to the seminal complex around Tb ion [86]. Similarly, the ferromagnetic interactions were observed between the Tb ion and radical ligand. Meanwhile, the complex also displays the temperature- and frequency-dependent χ'' signals below 6 K. However, a smaller effective barrier, $U_{\text{eff}} = 17$ K, was demonstrated under zero-dc applied

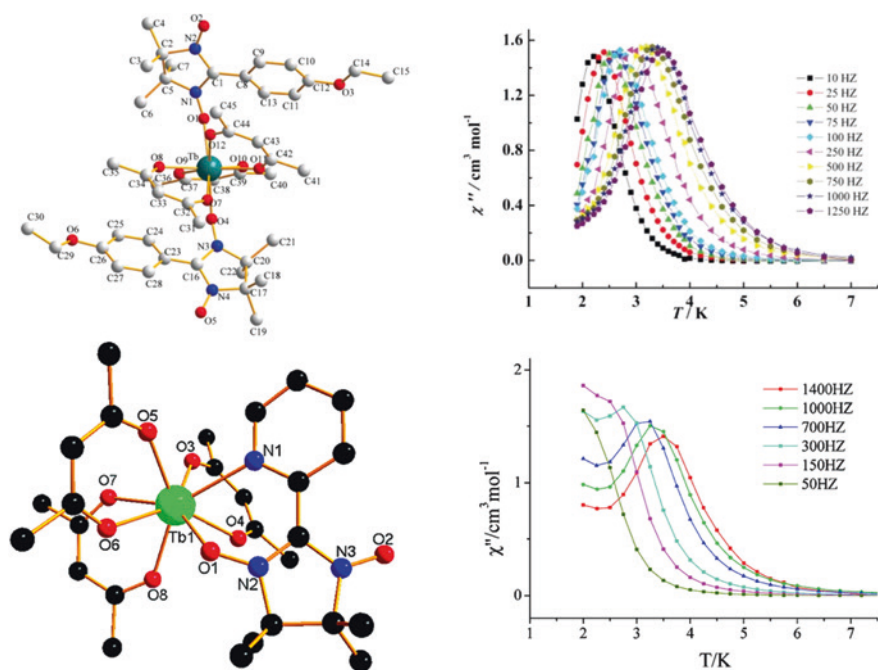


Fig. 2.33 The crystal structure and relaxation dynamics of two Tb β -diketone systems with NIT-R radical ligands. *Top* Reproduced from Ref. [85] by permission of The Royal Society of Chemistry. *Bottom* Reprinted with the permission from Ref. [86]. Copyright 2010 American Chemical Society

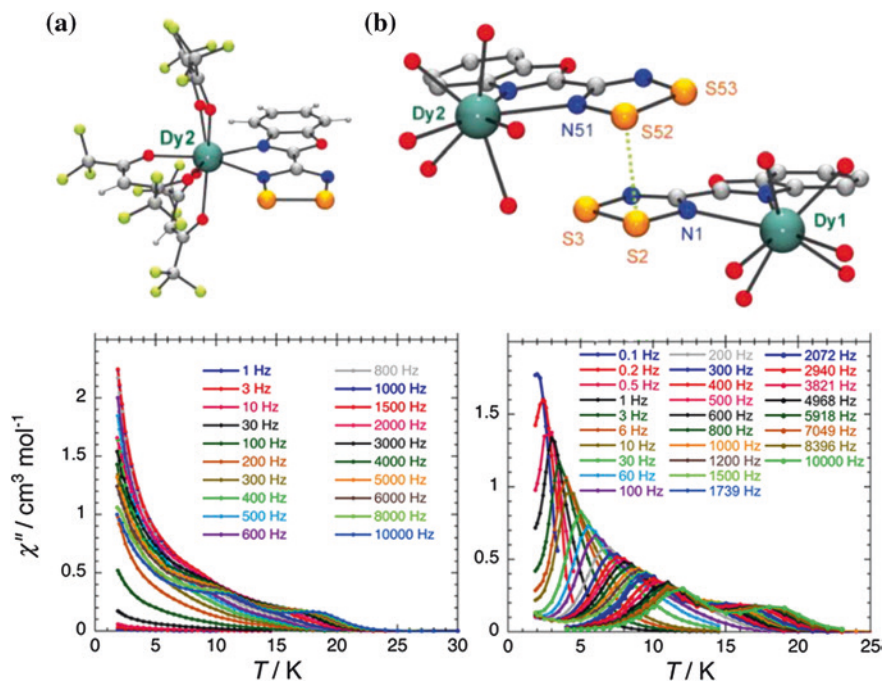


Fig. 2.34 The crystal structure and relaxation dynamics under zero- and nonzero-dc fields of Dy β -diketone systems with boaDTDA radical ligand. Reprinted with the permission from Ref. [94]. Copyright 2013 American Chemical Society

field. Here although the SMM properties are not so fascinating, it is a helpful exploration for the novel lanthanide-radical coupling system.

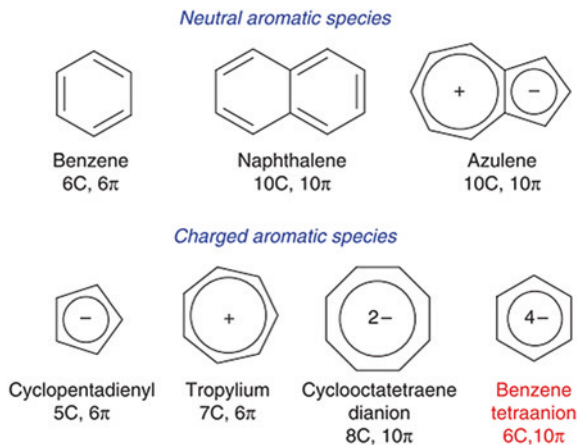
Furthermore, the new type of chelate radical ligand, 4-(benzoxazol-2'-yl)-1,2,3,5-dithiadiazolyl (boaDTDA in Fig. 2.21) [94], was also explored to construct the lanthanide-radical SMM system. As a result, a supramolecular species composed of a pair of non-equivalent Dy^{III}-radical complexes was obtained, as seen in Fig. 2.34, where two Dy ions are located in the different coordinate geometries, one being the distorted SAP geometry and the other being the dodecahedral geometry. In the molecular pairs, the close S–S contact leads to a *twisted-cofacial* interaction between two radical ligands, which further results in strong antiferromagnetic coupling between the DTDA radical spins. Obviously, the Dy complex exhibits the out-of-phase signals of ac susceptibility under zero-dc applied field, but the rapidly increasing χ'' values at low temperature are indicative of the presence of fast QTM relaxation, which may be related to the above antiferromagnetic coupling within the molecule pairs. Further, the application of a dc applied field leads to the occurrence of two relaxation processes (Fig. 2.34), which should correspond to the presence of two different metal centers in the complex. In particular, the almost same effective barriers were extracted to be 100 K for the two relaxation processes, but showing the different pre-exponential factors.

2.4 Organometallic SIMMs

To date, the most significant achievements in the SIMM field were present in the organometallic lanthanide SMMs, which exhibit not only the large effective barriers but also the very high blocking temperature (T_B) close to the T_B record achieved in the N_2^{3-} -bridged Tb_2 SMMs. Compared with the common O- or N-based coordination complexes, the organometallic systems provide alternative special chemical environments due to the applications of air-sensitive reagents with the extremely strong basicity, which potentially results in the stronger and more axial crystal field around lanthanide ions as well as thus the improved SMM properties [95]. In fact, the exploration into this aspect can date back to 2010 when an organometallic Dy_2 complex shows typical SMM behavior [96], but the mononuclear organometallic lanthanide SMMs were developed later. Now in the field, the most widely investigated species are the lanthanide systems coordinated by the negative-charged aromatic ligands, mainly cyclopentadienide (Cp^-) and cyclooctatetraene dianion (COT^{2-}) [9, 14, 20, 33], which exhibits the similar aromaticity to the neutral naphthalene and benzenoid compounds (Fig. 2.35) with the π electron cloud created by the multiple sp^2 carbon atoms [97]. The first reported example was $[(\eta^5-Cp^*)Er(\eta^8-COT)]$ SIMM [9] exhibiting the high effective barriers and blocking temperature, which further stimulates the researching interests in the new type of lanthanide SMM system. To date, the system has been extended well with the several important examples showing the high SMM performance, which achieves its celebrity status in the developments of SIMMs.

The first system, $[(Cp^*)Ln(COT)]$ ($Ln = Tb^{III}, Dy^{III}, Ho^{III}, Er^{III}, Tm^{III}, Y^{III}$, $Cp^* = C_5Me_5^-$; $COT = C_8H_8^{2-}$), was reported by S. Gao and coworkers since 2011 [9, 98]. The complex features the single lanthanide ion sandwiched by two unparallel aromatic ligands with a slight tilt angle, an important factor in determining the quantum tunneling relaxation time. Further research demonstrates

Fig. 2.35 The neutral and charged aromatic systems with the π electron cloud created by the multiple sp^2 carbon atoms. Reprinted by permission from Macmillan Publishers Ltd. Ref. [97], copyright 2013



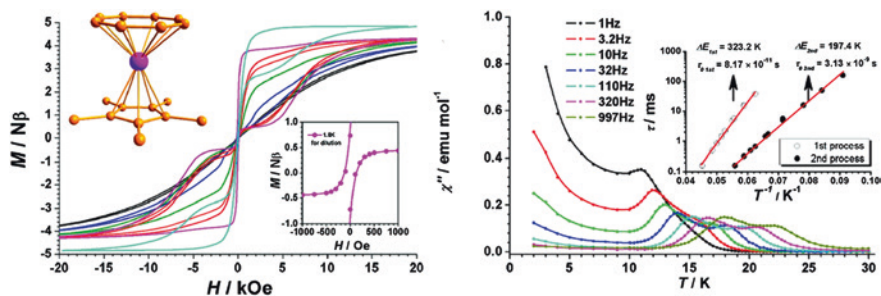


Fig. 2.36 The crystal structure and magnetic properties of $[(\text{Cp}^*)\text{Er}(\text{COT})]$. Reprinted with the permission from Ref. [9]. Copyright 2011 American Chemical Society

that the bending of the axis induced by asymmetric intermolecule interactions increases with the increment of ionic radius of lanthanide ions from Tm to Tb ions. Nevertheless, the sandwiched modes from two ligands with the high π -electron density are favorable to the strong axial anisotropy of lanthanide ions. Importantly, the ac susceptibility data reveal that the Er^{III} compound behaves as the better SIMM compared with other lanthanide complexes. Here, the out-of-phase signals in Fig. 2.36 demonstrate two clear maxima below 25 K indicating the two relaxation processes, as a possible result of the presence of two conformations in the crystal lattice. Therefore, two high effective barriers were given to be 323 and 197 K, which are among the highest effective barriers discovered to date. Further, the butterfly-shaped hysteresis loop with a coercive field was observed at 1.8 K, indicating the strongly blocking behavior for magnetic moments. Here, the strong SMM behavior mainly results from the strong single-ion anisotropy of Er ion, further leading to an Ising ground state well separated from other excited states, which has been confirmed by the recent angular-resolved magnetometry experiments and ab initio calculations [99]. Furthermore, both Dy^{III} and Ho^{III} compounds exhibit the field-induced SMM behavior.

Remarkably, two stronger Er-based SIMMs similar to above complex were obtained by J.R. Long group through applying the single aromatic ligand, COT^{2-} [33]. Here, both complexes contain the same part of $[\text{Er}(\text{COT})_2]^-$ with some slight differences and show the almost same static and dynamic magnetic properties. Therefore, only one example was described below, as shown in Fig. 2.37. Here, two almost coplanar COT^{2-} ligands lead to a higher symmetry close to D_{8h} in the $[\text{Er}(\text{COT})_2]^-$ part compared to the above $[(\text{Cp}^*)\text{Ln}(\text{COT})]$ complex. Dc magnetic susceptibility data reveal a precipitous drop of $\chi_m T$ values below 10 K indicating the strongly blocking of magnetization (Fig. 2.37). In order to further explore the magnetic blocking behavior, the ac magnetic susceptibility measurements were also performed, and therefore, the clear out-of-phase maxima are present below 27 K, which gives a effective barrier of 147 cm^{-1} (212 K). Most importantly, the hysteresis loops were observed below 10 K, which represents the highest blocking temperature yet observed for a mononuclear complex and the second highest for any single-molecule magnet. Nevertheless, as seen in most lanthanide SIMMs,

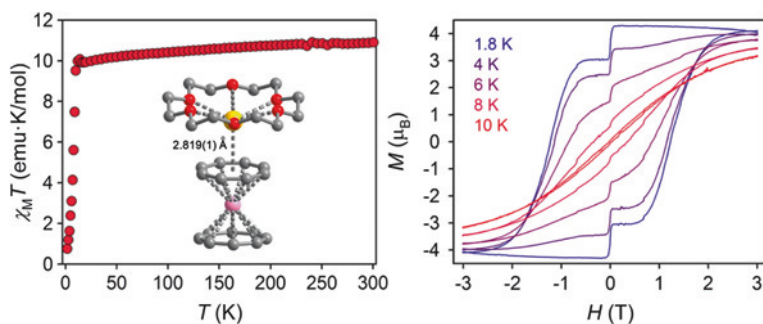


Fig. 2.37 The crystal structure and static magnetic properties of $[\text{Er}(\text{COT})_2]^-$. Reprinted with the permission from Ref. [33]. Copyright 2013 American Chemical Society

the magnetization in hysteresis loop still exhibits a sudden drop when approaching zero field, thus leading to the disappearance of coercive field. Further investigations indicate that such a drop mainly arise from the magnetic avalanche effects induced by intermolecular dipolar interactions. Therefore, the magnetic dilution for the above samples results in the obviously enhanced coercive field, and only a small drop of magnetization was observed at zero field, as seen in Fig. 2.37.

To further gain insight into the magnetic blocking mechanism in the molecule, L.F. Chibotaru et al. performed *ab initio* calculations for the Dy and Er complexes, as shown in Fig. 2.38 [20]. The results indicated that the local high symmetry for

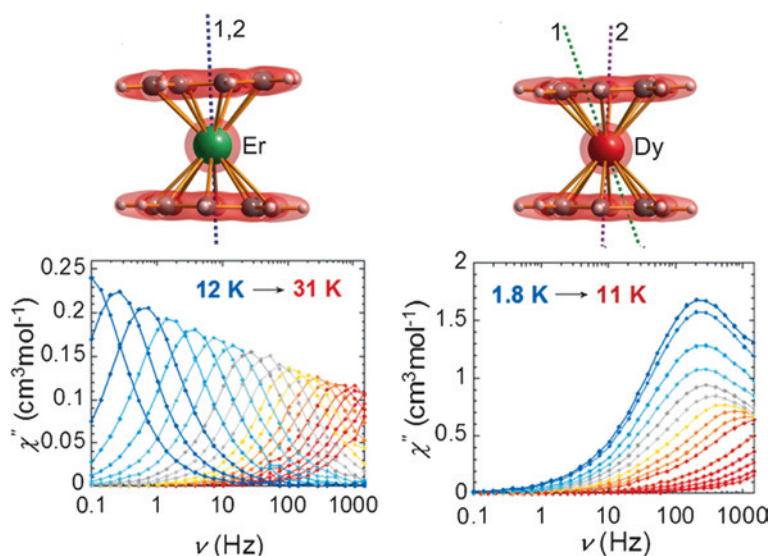


Fig. 2.38 The calculated anisotropic axes and relaxation dynamics of the Er and Dy complexes in $[\text{Er}(\text{COT})_2]^-$. Reproduced from Ref. [20] by permission of John Wiley & Sons Ltd.

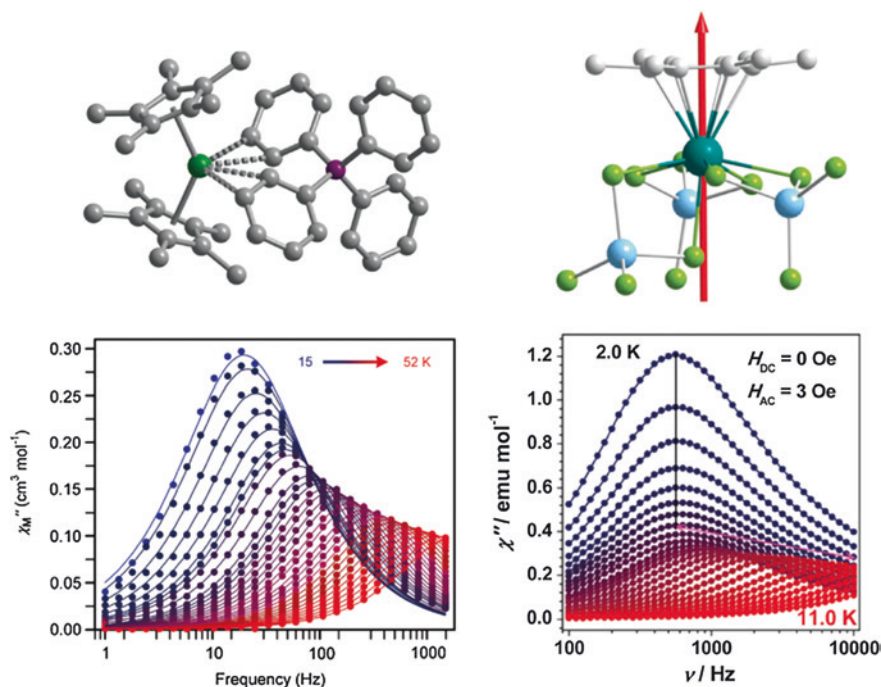


Fig. 2.39 The crystal structures and relaxation dynamics of $[\text{Cp}^*_2\text{Ln}(\text{BPh}_4)]$ from J.R. Long and $[(\text{C}_6\text{Me}_6)\text{Dy}(\text{AlCl}_4)_3]$ from S. Gao. *Left* Reproduced from Ref. [101] by permission of John Wiley & Sons Ltd. *Right* Reproduced from Ref. [102] by permission of The Royal Society of Chemistry

the Er complex plays an extremely crucial role in promoting the magnetic relaxation and suppressing the QTM. In the Er complex, the ground state is well separated from the low-lying excited states and, importantly, the ground and first excited Kramers doublets exhibit the strong uniaxial anisotropy and almost collinear anisotropy axes, thus leading to the magnetic relaxation pathway via second excited state. By contrast, the corresponding Dy analogue exhibits the weak SMM behavior, which is mainly due to the low ground state and fast QTM arising from the large transversal components. Further, the determination of crystal parameters gives a reasonable explanation for such a large difference. The important negative crystal parameters B_2^0 and B_4^0 in the Er complex reveal the stronger equatorial component of the ligand field than the axial one, which supports the easy axis anisotropy and the large spin ground state for the Er ion, while the opposite case occurs in Dy complex. In addition, the trimethylsilyl substituted Dy and Er species reported by M. Murugesu exhibit similar SMM properties [100].

Recently, the J. R. Long and S. Gao groups explored the low-symmetric organometallic lanthanide systems, as shown in Fig. 2.39, both of which exhibit the typical SMM properties. In particular, for the first system, $[\text{Cp}^*_2\text{Ln}(\text{BPh}_4)]$ ($\text{Ln} = \text{Tb}$ and Dy) [101], the Dy species shows the strongly magnetic blocking behavior, as

evidenced by the high blocking temperature up to 52 K characterized by the out-of-phase signals of ac susceptibility data in Fig. 2.39. Further, the effective barrier was extracted to be 331 cm^{-1} (477 K), which is of the highest known for the mononuclear Dy-based SMMs. Meanwhile, the Tb analogue also exhibits the robust field-induced SMM behavior with a large effective barrier of 216 cm^{-1} (311 K). Here, the authors attributed their large barriers to the bent ligand field presented to the Ln^{III} centers due to the weak interactions between the lanthanide ions and BPh_4^- anion. The second example, $[(\text{C}_6\text{Me}_6)\text{Dy}(\text{AlCl}_4)_3]$, reported by S. Gao et al. [102] demonstrates a half-sandwich structure with the coordination of a neutral π -bonded arene ligand to Dy ion. An effective barrier of 101 K was present in the complex under zero-dc applied field, which mainly arises from the strong single-ion anisotropy of Dy ion indicated by the ab initio calculations. Finally, it is noted that in spite of the high barriers the fast tunneling relaxation is clearly present in those complexes compared with the above double-decker organometallic complexes, which is as a main result of the internal low-symmetric factors of local crystal field.

2.5 Conclusion

The most important lanthanide SIMM systems including the lanthanide phthalocyanine, lanthanide β -diketone, and organometallic lanthanide systems have been reviewed in detail in this chapter. Here, we provide a clear guideline for designing the effective SMMs in each class through systematically discussing the corresponding lanthanide SIMMs discovered to date. In addition, some low-symmetric lanthanide complexes with the local axial coordination geometries around lanthanide ions which also behave as typical SMMs even with the very high effective barriers are not discussed here. Undoubtedly, the lanthanide SIMM is the most important class in the development of SMM to date; for that, they play an outstanding role not only in the assembly of lanthanide SMMs with high effective barriers and blocking temperature, but also in elucidating the correlation between the magnetic properties and the structural features. In particular, both the previous $[\text{LnPc}_2]$ complexes and the recently discovered lanthanide organometallic complexes demonstrate the great potential in further promoting the SMM properties and the future technological applications as quantum bits.

References

1. Miller JS (2011) Magnetically ordered molecule-based materials. *Chem Soc Rev* 40(6):3266–3296. doi:[10.1039/c0cs00166j](https://doi.org/10.1039/c0cs00166j)
2. Miller JS, Epstein AJ (2000) Molecule-based magnets-an overview. *MRS Bull* 25(11):21–30
3. Sun H-L, Wang Z-M, Gao S (2010) Strategies towards single-chain magnets. *Coord Chem Rev* 254(9–10):1081–1100. doi:[10.1016/j.ccr.2010.02.010](https://doi.org/10.1016/j.ccr.2010.02.010)

4. Miyasaka H, Julve M, Yamashita M et al (2009) Slow dynamics of the magnetization in one-dimensional coordination polymers: single-chain magnets. *Inorg Chem* 48(8):3420–3437. doi:[10.1021/ic802050j](https://doi.org/10.1021/ic802050j)
5. Christou G, Gatteschi D, Hendrickson DN et al (2000) Single-molecule magnets. *MRS Bull* 25(11):66–71. doi:[10.1557/mrs2000.204](https://doi.org/10.1557/mrs2000.204)
6. Bernot K, Luzon J, Bogani L et al (2009) Magnetic anisotropy of dysprosium(III) in a low-symmetry environment: a theoretical and experimental investigation. *J Am Chem Soc* 131(15):5573–5579. doi:[10.1021/ja8100038](https://doi.org/10.1021/ja8100038)
7. Rinehart JD, Fang M, Evans WJ et al (2011) Strong exchange and magnetic blocking in N_2^{3-} -radical-bridged lanthanide complexes. *Nat Chem* 3(7):538–542. doi:[10.1038/nchem.1063](https://doi.org/10.1038/nchem.1063)
8. Jiang SD, Wang BW, Su G et al (2010) A mononuclear dysprosium complex featuring single-molecule-magnet behavior. *Angew Chem Int Ed* 49:7448–7451. doi:[10.1002/anie.201004027](https://doi.org/10.1002/anie.201004027)
9. Jiang S-D, Wang B-W, Sun H-L et al (2011) An organometallic single-ion magnet. *J Am Chem Soc* 133(13):4730–4733. doi:[10.1021/ja200198v](https://doi.org/10.1021/ja200198v)
10. Feltham HLC, Brooker S (2014) Review of purely 4f and mixed-metal *nd-4f* single-molecule magnets containing only one lanthanide ion. *Coord Chem Rev* 276:1–33. doi:[10.1016/j.ccr.2014.05.011](https://doi.org/10.1016/j.ccr.2014.05.011)
11. Ishikawa N, Sugita M, Ishikawa T et al (2003) Lanthanide double-decker complexes functioning as magnets at the single-molecular level. *J Am Chem Soc* 125(29):8694–8695. doi:[10.1021/ja029629n](https://doi.org/10.1021/ja029629n)
12. AlDamen MA, Clemente-Juan JM, Coronado E et al (2008) Mononuclear lanthanide single-molecule magnets based on polyoxometalates. *J Am Chem Soc* 130(28):8874–8875. doi:[10.1021/ja801659m](https://doi.org/10.1021/ja801659m)
13. Chen G-J, Guo Y-N, Tian J-L et al (2012) Enhancing anisotropy barriers of dysprosium(III) single-ion magnets. *Chem Eur J* 18(9):2484–2487. doi:[10.1002/chem.201103816](https://doi.org/10.1002/chem.201103816)
14. Jeletic M, Lin P-H, Le Roy JJ et al (2011) An organometallic sandwich lanthanide single-ion magnet with an unusual multiple relaxation mechanism. *J Am Chem Soc* 133(48):19286–19289. doi:[10.1021/ja207891y](https://doi.org/10.1021/ja207891y)
15. Freedman DE, Harman WH, Harris TD et al (2010) Slow magnetic relaxation in a high-spin iron(II) complex. *J Am Chem Soc* 132(4):1224–1225. doi:[10.1021/ja909560d](https://doi.org/10.1021/ja909560d)
16. Zadrozny JM, Long JR (2011) Slow magnetic relaxation at zero field in the tetrahedral complex $[\text{Co}(\text{SPh})_4]^{2-}$. *J Am Chem Soc* 133(51):20732–20734. doi:[10.1021/ja2100142](https://doi.org/10.1021/ja2100142)
17. Zadrozny JM, Xiao DJ, Atanasov M et al (2013) Magnetic blocking in a linear iron(I) complex. *Nat Chem* 5(7):577–581. doi:[10.1038/nchem.1630](https://doi.org/10.1038/nchem.1630)
18. Rinehart JD, Long JR (2009) Slow magnetic relaxation in a trigonal prismatic uranium(III) complex. *J Am Chem Soc* 131(35):12558–12559. doi:[10.1021/ja906012u](https://doi.org/10.1021/ja906012u)
19. Magnani N, Apostolidis C, Morgenstern A et al (2011) Magnetic memory effect in a transuranic mononuclear complex. *Angew Chem Int Ed* 50(7):1696–1698. doi:[10.1002/anie.201006619](https://doi.org/10.1002/anie.201006619)
20. Ungur L, Le Roy JJ, Korobkov I et al (2014) Fine-tuning the local symmetry to attain record blocking temperature and magnetic remanence in a single-ion magnet. *Angew Chem Int Ed* 53(17):4413–4417. doi:[10.1002/anie.201310451](https://doi.org/10.1002/anie.201310451)
21. Zhang P, Zhang L, Wang C et al (2014) Equatorially coordinated lanthanide single ion magnets. *J Am Chem Soc* 136(12):4484–4487. doi:[10.1021/ja500793x](https://doi.org/10.1021/ja500793x)
22. Watanabe A, Yamashita A, Nakano M et al (2011) Multi-path magnetic relaxation of mono-dysprosium(III) single-molecule magnet with extremely high barrier. *Chem Eur J* 17(27):7428–7432. doi:[10.1002/chem.201003538](https://doi.org/10.1002/chem.201003538)
23. Rinehart JD, Long JR (2011) Exploiting single-ion anisotropy in the design of f-element single-molecule magnets. *Chem Sci* 2(11):2078–2085. doi:[10.1039/C1SC00513H](https://doi.org/10.1039/C1SC00513H)
24. Cucinotta G, Perfetti M, Luzon J et al (2012) Magnetic anisotropy in a dysprosium/DOTA single-molecule magnet: beyond simple magneto-structural correlations. *Angew Chem Int Ed* 51(7):1606–1610. doi:[10.1002/anie.201107453](https://doi.org/10.1002/anie.201107453)

25. Boulon M-E, Cucinotta G, Luzon J et al (2013) Magnetic anisotropy and spin-parity effect along the series of lanthanide complexes with DOTA. *Angew Chem Int Ed* 52(1):350–354. doi:[10.1002/anie.201205938](#)
26. Meihäus KR, Minasian SG, Lukens WW et al (2014) Influence of pyrazolate vs N-heterocyclic carbene ligands on the slow magnetic relaxation of homoleptic trischelate lanthanide(III) and uranium(III) complexes. *J Am Chem Soc* 136(16):6056–6068. doi:[10.1021/ja501569t](#)
27. Benelli C, Gatteschi D (2002) Magnetism of lanthanides in molecular materials with transition-metal ions and organic radicals. *Chem Rev* 102(6):2369–2388. doi:[10.1021/cr010303r](#)
28. Skomski R (2008) Simple models of magnetism. Oxford University Press, New York
29. Zhang P, Guo Y-N, Tang J (2013) Recent advances in dysprosium-based single molecule magnets: structural overview and synthetic strategies. *Coord Chem Rev* 257(11–12):1728–1763. doi:[10.1016/j.ccr.2013.01.012](#)
30. Ungur L, Chibotaru LF (2011) Magnetic anisotropy in the excited states of low symmetry lanthanide complexes. *Phys Chem Chem Phys* 13(45):20086–20090. doi:[10.1039/C1CP22689D](#)
31. Ishikawa N, Sugita M, Wernsdorfer W (2005) Quantum tunneling of magnetization in lanthanide single-molecule magnets: bis(phthalocyaninato)terbium and bis(phthalocyaninato) dysprosium anions. *Angew Chem Int Ed* 44(19):2931–2935. doi:[10.1002/anie.200462638](#)
32. da Cunha TT, Jung J, Boulon M-E et al (2013) Magnetic poles determinations and robustness of memory effect upon solubilization in a Dy^{III}-based single ion magnet. *J Am Chem Soc* 135(44):16332–16335. doi:[10.1021/ja4089956](#)
33. Meihäus KR, Long JR (2013) Magnetic blocking at 10 K and a dipolar-mediated avalanche in salts of the bis(η^8 -cyclooctatetraenide) complex [Er(COT)₂][−]. *J Am Chem Soc* 135(47):17952–17957. doi:[10.1021/ja4094814](#)
34. Guo Y-N, Ungur L, Granroth GE et al (2014) An NCN-pincer ligand dysprosium single-ion magnet showing magnetic relaxation via the second excited state. *Sci Rep* 4:5471. doi:[10.1038/srep05471](#)
35. Sorace L, Benelli C, Gatteschi D (2011) Lanthanides in molecular magnetism: old tools in a new field. *Chem Soc Rev* 40(6):3092–3104. doi:[10.1039/C0CS00185F](#)
36. Liu J-L, Chen Y-C, Zheng Y-Z et al (2013) Switching the anisotropy barrier of a single-ion magnet by symmetry change from quasi-D_{5h} to quasi-O_h. *Chem Sci* 4(8):3310–3316. doi:[10.1039/c3sc50843a](#)
37. Baldoví JJ, Cardona-Serra S, Clemente-Juan JM et al (2012) Rational design of single-ion magnets and spin qubits based on mononuclear lanthanoid complexes. *Inorg Chem* 51(22):12565–12574. doi:[10.1021/ic302068c](#)
38. Görlner-Walrand C, Binnemans K (1996) Rationalization of crystal-field parametrization Chap. 155. In: Gschneidner KA Jr, LeRoy E (eds) *Handbook on the physics and chemistry of rare earths*, vol 23. Elsevier, Amsterdam, pp 121–283. doi:[10.1016/S0168-1273\(96\)23006-5](#)
39. Dolbecq A, Dumas E, Mayer CR et al (2010) Hybrid organic–inorganic polyoxometalate compounds: from structural diversity to applications. *Chem Rev* 110(10):6009–6048. doi:[10.1021/cr1000578](#)
40. Huang C (2010) Rare earth coordination chemistry: fundamentals and applications. John Wiley & Sons (Asia) Pte Ltd. Singapore
41. Ishikawa N (2010) Phthalocyanine-based magnets. In: Jiang J (ed) *Functional phthalocyanine molecular materials*, vol 135. Structure and bonding. Springer, Berlin, pp 211–228. doi:[10.1007/978-3-642-04752-7_7](#)
42. Takamatsu S, Ishikawa T, Koshihara S et al (2007) Significant increase of the barrier energy for magnetization reversal of a single-4f-ionic single-molecule magnet by a longitudinal contraction of the coordination space. *Inorg Chem* 46(18):7250–7252. doi:[10.1021/ic700954t](#)
43. De Cian A, Moussavi M, Fischer J et al (1985) Synthesis, structure, and spectroscopic and magnetic properties of lutetium(III) phthalocyanine derivatives: LuPc₂·CH₂Cl₂ and [LuPc(OAc)(H₂O)₂]·H₂O·2CH₃OH. *Inorg Chem* 24(20):3162–3167. doi:[10.1021/ic00214a016](#)

44. Ishikawa N, Sugita M, Okubo T et al (2003) Determination of ligand-field parameters and f-electronic structures of double-decker bis(phthalocyaninato)lanthanide complexes. *Inorg Chem* 42(7):2440–2446. doi:[10.1021/ic026295u](https://doi.org/10.1021/ic026295u)
45. Thomas L, Lioni F, Ballou R et al (1996) Macroscopic quantum tunnelling of magnetization in a single crystal of nanomagnets. *Nature* 383(6596):145–147. doi:[10.1038/383145a0](https://doi.org/10.1038/383145a0)
46. Ishikawa N, Sugita M, Wernsdorfer W (2005) Nuclear spin driven quantum tunneling of magnetization in a new lanthanide single-molecule magnet: bis(phthalocyaninato)holmium anion. *J Am Chem Soc* 127(11):3650–3651. doi:[10.1021/ja0428661](https://doi.org/10.1021/ja0428661)
47. Ishikawa N, Ohno O, Kaizu Y (1993) Electronic states of bis(phthalocyaninato)lutetium radical and its related compounds: the application of localized orbital basis set to open-shell phthalocyanine dimers. *J Phys Chem* 97(5):1004–1010. doi:[10.1021/j100107a006](https://doi.org/10.1021/j100107a006)
48. Takamatsu S, Ishikawa N (2007) A theoretical study of a drastic structural change of bis(phthalocyaninato)lanthanide by ligand oxidation: towards control of ligand field strength and magnetism of single-lanthanide-ionic single molecule magnet. *Polyhedron* 26(9–11):1859–1862. doi:[10.1016/j.poly.2006.09.020](https://doi.org/10.1016/j.poly.2006.09.020)
49. Ishikawa N, Sugita M, Tanaka N et al (2004) Upward temperature shift of the intrinsic phase lag of the magnetization of bis(phthalocyaninato)terbium by ligand oxidation creating an $S = 1/2$ spin. *Inorg Chem* 43(18):5498–5500. doi:[10.1021/ic049348b](https://doi.org/10.1021/ic049348b)
50. Ishikawa N, Mizuno Y, Takamatsu S et al (2008) Effects of chemically induced contraction of a coordination polyhedron on the dynamical magnetism of bis(phthalocyaninato)disprosium, a single-4f-ionic single-molecule magnet with a Kramers ground state. *Inorg Chem* 47(22):10217–10219. doi:[10.1021/ic8014892](https://doi.org/10.1021/ic8014892)
51. Gonidec M, Davies ES, McMaster J et al (2010) Probing the magnetic properties of three interconvertible redox states of a single-molecule magnet with magnetic circular dichroism spectroscopy. *J Am Chem Soc* 132(6):1756–1757. doi:[10.1021/ja9095895](https://doi.org/10.1021/ja9095895)
52. McInnes EJJ, Pidcock E, Oganessian VS et al (2002) Optical detection of spin polarization in single-molecule magnets $[\text{Mn}_{12}\text{O}_{12}(\text{O}_2\text{CR})_{16}(\text{H}_2\text{O})_4]$. *J Am Chem Soc* 124(31):9219–9228. doi:[10.1021/ja020456b](https://doi.org/10.1021/ja020456b)
53. Gonidec M, Krivokapic I, Vidal-Gancedo J et al (2013) Highly reduced double-decker single-molecule magnets exhibiting slow magnetic relaxation. *Inorg Chem* 52(8):4464–4471. doi:[10.1021/ic3027418](https://doi.org/10.1021/ic3027418)
54. Ganiwet CR, Ballesteros B, de la Torre G et al (2013) Influence of peripheral substitution on the magnetic behavior of single-ion magnets based on homo- and heteroleptic Tb^{III} bis(phthalocyaninate). *Chem Eur J* 19(4):1457–1465. doi:[10.1002/chem.201202600](https://doi.org/10.1002/chem.201202600)
55. Gonidec M, Luis F, Vilchez Á et al (2010) A liquid-crystalline single-molecule magnet with variable magnetic properties. *Angew Chem Int Ed* 49(9):1623–1626. doi:[10.1002/ange.200905007](https://doi.org/10.1002/ange.200905007)
56. Gonidec M, Amabilino DB, Veciana J (2012) Novel double-decker phthalocyaninato terbium(III) single molecule magnets with stabilised redox states. *Dalton Trans* 41(44):13632–13639. doi:[10.1039/c2dt31171b](https://doi.org/10.1039/c2dt31171b)
57. Katoh K, Isshiki H, Komeda T et al (2011) Multiple-decker phthalocyaninato $\text{Tb}(\text{III})$ single-molecule magnets and $\text{Y}(\text{III})$ complexes for next generation devices. *Coord Chem Rev* 255(17–18):2124–2148. doi:[10.1016/j.ccr.2011.02.024](https://doi.org/10.1016/j.ccr.2011.02.024)
58. Katoh K, Umetsu K, Breedlove Brian K et al (2012) Magnetic relaxation behavior of a spatially closed dysprosium(III) phthalocyaninato double-decker complex. *Sci China Chem* 55(6):918–925. doi:[10.1007/s11426-012-4615-9](https://doi.org/10.1007/s11426-012-4615-9)
59. Waters M, Moro F, Krivokapic I et al (2012) Synthesis, characterisation and magnetic study of a cyano-substituted dysprosium double decker single-molecule magnet. *Dalton Trans* 41(4):1128–1130. doi:[10.1039/c1dt11880c](https://doi.org/10.1039/c1dt11880c)
60. Tanaka D, Inose T, Tanaka H et al (2012) Proton-induced switching of the single molecule magnetic properties of a porphyrin based Tb^{III} double-decker complex. *Chem Commun* 48(63):7796–7798. doi:[10.1039/c2cc00086e](https://doi.org/10.1039/c2cc00086e)

61. Wang H, Wang K, Tao J et al (2012) Twist angle perturbation on mixed (phthalocyaninato) (porphyrinato) dysprosium(III) double-decker SMMs. *Chem Commun* 48(24):2973–2975. doi:[10.1039/c2cc16543k](https://doi.org/10.1039/c2cc16543k)
62. Williams UJ, Mahoney BD, DeGregorio PT et al (2012) A comparison of the effects of symmetry and magnetoanisotropy on paramagnetic relaxation in related dysprosium single ion magnets. *Chem Commun* 48(45):5593–5595. doi:[10.1039/c2cc31227a](https://doi.org/10.1039/c2cc31227a)
63. AlDamen MA, Cardona-Serra S, Clemente-Juan JM et al (2009) Mononuclear lanthanide single molecule magnets based on the polyoxometalates $[\text{Ln}(\text{W}_5\text{O}_{18})_2]^{9-}$ and $[\text{Ln}(\beta_2\text{-SiW}_{11}\text{O}_{39})_2]^{13-}$ ($\text{Ln}^{\text{III}} = \text{Tb, Dy, Ho, Er, Tm, and Yb}$). *Inorg Chem* 48(8):3467–3479. doi:[10.1021/ic801630z](https://doi.org/10.1021/ic801630z)
64. Cardona-Serra S, Clemente-Juan JM, Coronado E et al (2012) Lanthanoid single-ion magnets based on polyoxometalates with a 5-fold symmetry: the series $[\text{LnP}_5\text{W}_{30}\text{O}_{110}]^{12-}$ ($\text{Ln}^{3+} = \text{Tb, Dy, Ho, Er, Tm, and Yb}$). *J Am Chem Soc* 134(36):14982–14990. doi:[10.1021/ja305163t](https://doi.org/10.1021/ja305163t)
65. Bogani L, Sangregorio C, Sessoli R et al (2005) Molecular engineering for single-chain-magnet behavior in a one-dimensional dysprosium-nitronyl nitroxide compound. *Angew Chem Int Ed* 44(36):5817–5821. doi:[10.1002/anie.200500464](https://doi.org/10.1002/anie.200500464)
66. Aravena D, Ruiz E (2013) Shedding light on the single-molecule magnet behavior of mononuclear Dy^{III} complexes. *Inorg Chem* 52(23):13770–13778. doi:[10.1021/ic402367c](https://doi.org/10.1021/ic402367c)
67. Chilton NF, Collison D, McInnes EJJ et al (2013) An electrostatic model for the determination of magnetic anisotropy in dysprosium complexes. *Nat Commun* 4:2551. doi:[10.1038/ncomms3551](https://doi.org/10.1038/ncomms3551)
68. Bi Y, Guo Y-N, Zhao L et al (2011) Capping ligand perturbed slow magnetic relaxation in dysprosium single-ion magnets. *Chem Eur J* 17(44):12476–12481. doi:[10.1002/chem.201101838](https://doi.org/10.1002/chem.201101838)
69. Wang Y-L, Gu B, Ma Y et al (2014) A new D_{2d} -symmetry Dy^{III} mononuclear single-molecule magnet containing a monodentate N-heterocyclic donor ligand. *CrystEngComm* 16(11):2283–2289. doi:[10.1039/c3ce42212g](https://doi.org/10.1039/c3ce42212g)
70. Cao D-K, Gu Y-W, Feng J-Q et al (2013) Mononuclear lanthanide complexes incorporating an anthracene group: structural modification, slow magnetic relaxation and multicomponent fluorescence emissions in Dy compounds. *Dalton Trans* 42(32):11436–11444. doi:[10.1039/c3dt51176f](https://doi.org/10.1039/c3dt51176f)
71. Wang Y-L, Ma Y, Yang X et al (2013) Syntheses, structures, and magnetic and luminescence properties of a new Dy^{III} -based single-ion magnet. *Inorg Chem* 52(13):7380–7386. doi:[10.1021/ic400006n](https://doi.org/10.1021/ic400006n)
72. Silva MR, Martin-Ramos P, Coutinho JT et al (2014) Effect of the capping ligand on luminescent erbium(III) β -diketonate single-ion magnets. *Dalton Trans* 43(18):6752–6761. doi:[10.1039/c4dt00168k](https://doi.org/10.1039/c4dt00168k)
73. Li X-L, Chen C-L, Gao Y-L et al (2012) Modulation of homochiral Dy^{III} complexes: single-molecule magnets with ferroelectric properties. *Chem Eur J* 18(46):14632–14637. doi:[10.1002/chem.201201190](https://doi.org/10.1002/chem.201201190)
74. Li D-P, Zhang X-P, Wang T-W et al (2011) Distinct magnetic dynamic behavior for two polymorphs of the same $\text{Dy}(\text{III})$ complex. *Chem Commun* 47(24):6867–6869. doi:[10.1039/C1CC11659B](https://doi.org/10.1039/C1CC11659B)
75. Li D-P, Wang T-W, Li C-H et al (2010) Single-ion magnets based on mononuclear lanthanide complexes with chiral schiff base ligands $[\text{Ln}(\text{FTA})_3\text{L}]$ ($\text{Ln} = \text{Sm, Eu, Gd, Tb and Dy}$). *Chem Commun* 46(17):2929–2931. doi:[10.1039/B924547B](https://doi.org/10.1039/B924547B)
76. Wang Y, Li X-L, Wang T-W et al (2009) Slow relaxation processes and single-ion magnetic behaviors in dysprosium-containing complexes. *Inorg Chem* 49(3):969–976. doi:[10.1021/ic901720a](https://doi.org/10.1021/ic901720a)
77. Liu C-M, Zhang D-Q, Zhu D-B (2013) Field-induced single-ion magnets based on enantiopure chiral β -diketonate ligands. *Inorg Chem* 52(15):8933–8940. doi:[10.1021/ic4011218](https://doi.org/10.1021/ic4011218)

78. Coronado E, Galan-Mascaros JR, Gomez-Garcia CJ et al (2000) Coexistence of ferromagnetism and metallic conductivity in a molecule-based layered compound. *Nature* 408(6811):447–449. doi:[10.1038/35044035](https://doi.org/10.1038/35044035)
79. Kubo K, Shiga T, Yamamoto T et al (2011) Electronic state of a conducting single molecule magnet based on Mn-salen type and Ni-dithiolene complexes. *Inorg Chem* 50(19): 9337–9344. doi:[10.1021/ic200863c](https://doi.org/10.1021/ic200863c)
80. Pointillart F, Le Gal Y, Golhen S et al (2011) Single-molecule magnet behaviour in a tetrathiafulvalene-based electroactive antiferromagnetically coupled dinuclear dysprosium(III) complex. *Chem Eur J* 17(37):10397–10404. doi:[10.1002/chem.201100869](https://doi.org/10.1002/chem.201100869)
81. Di Piazza E, Norel L, Costuas K et al (2011) *d-f* Heterobimetallic association between ytterbium and ruthenium carbon-rich complexes: redox commutation of near-IR luminescence. *J Am Chem Soc* 133(16):6174–6176. doi:[10.1021/ja2023515](https://doi.org/10.1021/ja2023515)
82. Norel L, Feng M, Bernot K et al (2014) Redox modulation of magnetic slow relaxation in a 4f-based single-molecule magnet with a 4d carbon-rich ligand. *Inorg Chem* 53(5):2361–2363. doi:[10.1021/ic403081y](https://doi.org/10.1021/ic403081y)
83. Norel L, Bernot K, Feng M et al (2012) A carbon-rich ruthenium decorated dysprosium single molecule magnet. *Chem Commun* 48(33):3948–3950. doi:[10.1039/c2cc30604b](https://doi.org/10.1039/c2cc30604b)
84. Woodruff DN, Winpenny REP, Layfield RA (2013) Lanthanide single-molecule magnets. *Chem Rev* 113:5110–5148. doi:[10.1021/cr400018q](https://doi.org/10.1021/cr400018q)
85. Zhou N, Ma Y, Wang C et al (2009) A monometallic tri-spin single-molecule magnet based on rare earth radicals. *Dalton Trans* 40:8489–8492. doi:[10.1039/b908639k](https://doi.org/10.1039/b908639k)
86. Wang X-L, Li L-C, Liao D-Z (2010) Slow magnetic relaxation in lanthanide complexes with chelating nitronyl nitroxide radical. *Inorg Chem* 49(11):4735–4737. doi:[10.1021/ic100008g](https://doi.org/10.1021/ic100008g)
87. Bernot K, Pointillart F, Rosa P et al (2010) Single molecule magnet behaviour in robust dysprosium-biradical complexes. *Chem Commun* 46(35):6458–6460. doi:[10.1039/c0cc00966k](https://doi.org/10.1039/c0cc00966k)
88. Wang X, Bao X, Xu P et al (2011) From discrete molecule to one-dimension chain: two new nitronyl nitroxide–lanthanide complexes exhibiting slow magnetic relaxation. *Eur J Inorg Chem* 2011(24):3586–3591. doi:[10.1002/ejic.201100296](https://doi.org/10.1002/ejic.201100296)
89. Mei X-L, Ma Y, Li L-C et al (2012) Ligand field-tuned single-molecule magnet behaviour of 2p-4f complexes. *Dalton Trans* 41:505–511. doi:[10.1039/C1DT11795E](https://doi.org/10.1039/C1DT11795E)
90. Wang X-L, Tian H-X, Ma Y et al (2011) Slow magnetic relaxation in lanthanide complexes with chelating imino nitroxide radicals. *Inorg Chem Commun* 14(11):1728–1731. doi:[10.1016/j.inoche.2011.07.016](https://doi.org/10.1016/j.inoche.2011.07.016)
91. Hu P, Zhu M, Mei X et al (2012) Single-molecule magnets based on rare earth complexes with chelating benzimidazole-substituted nitronyl nitroxide radicals. *Dalton Trans* 41(48):14651–14656. doi:[10.1039/c2dt31806g](https://doi.org/10.1039/c2dt31806g)
92. Tian L, Sun Y-Q, Na B et al (2013) A family of homologous heterospin complexes based on lanthanides and biradical ligands. *Eur J Inorg Chem* 2013(24):4329–4335. doi:[10.1002/ejic.201300524](https://doi.org/10.1002/ejic.201300524)
93. Coronado E, Giménez-Saiz C, Recueno A et al (2011) Single-molecule magnetic behavior in a neutral terbium(III) complex of a picolinate-based nitronyl nitroxide free radical. *Inorg Chem* 50(16):7370–7372. doi:[10.1021/ic2010425](https://doi.org/10.1021/ic2010425)
94. Fatila EM, Rouzières M, Jennings MC et al (2013) Fine-tuning the single-molecule magnet properties of a [Dy(III)-radical]₂ pair. *J Am Chem Soc* 135(26):9596–9599. doi:[10.1021/ja403794d](https://doi.org/10.1021/ja403794d)
95. Layfield RA (2014) Organometallic single-molecule magnets. *Organometallics* 33(5):1084–1099. doi:[10.1021/om401107f](https://doi.org/10.1021/om401107f)
96. Layfield RA, McDouall JJW, Sulway SA et al (2010) Influence of the N-bridging ligand on magnetic relaxation in an organometallic dysprosium single-molecule magnet. *Chem Eur J* 16(15):4442–4446. doi:[10.1002/chem.201000158](https://doi.org/10.1002/chem.201000158)
97. Huang W, Dulong F, Wu T et al (2013) A six-carbon 10π-electron aromatic system supported by group 3 metals. *Nat Commun* 4:1448. doi:[10.1038/ncomms2473](https://doi.org/10.1038/ncomms2473)

98. Jiang S-D, Liu S-S, Zhou L-N et al (2012) Series of lanthanide organometallic single-ion magnets. *Inorg Chem* 51(5):3079–3087. doi:[10.1021/ic202511n](https://doi.org/10.1021/ic202511n)
99. Boulon M-E, Cucinotta G, Liu S-S et al (2013) Angular-resolved magnetometry beyond triclinic crystals: out-of-equilibrium studies of Cp*ErCOT single-molecule magnet. *Chem Eur J* 19(41):13726–13731. doi:[10.1002/chem.201302600](https://doi.org/10.1002/chem.201302600)
100. Le Roy JJ, Korobkov I, Murugesu M (2014) A sandwich complex with axial symmetry for harnessing the anisotropy in a prolate erbium(III) ion. *Chem Commun* 50(13):1602–1604. doi:[10.1039/c3cc48557a](https://doi.org/10.1039/c3cc48557a)
101. Demir S, Zadrozny JM, Long JR (2014) Large spin-relaxation barriers for the low-symmetry organolanthanide complexes [Cp*₂Ln(BPh₄)] (Cp* = pentamethylcyclopentadienyl; Ln = Tb, Dy). *Chem Eur J* 20(31):9524–9529. doi:[10.1002/chem.201403751](https://doi.org/10.1002/chem.201403751)
102. Liu S-S, Ziller JW, Zhang Y-Q et al (2014) A half-sandwich organometallic single-ion magnet with hexamethylbenzene coordinated to the Dy(III) ion. *Chem Commun* 50(77):11418–11420. doi:[10.1039/c4cc04262j](https://doi.org/10.1039/c4cc04262j)

Lanthanide Single Molecule Magnets

Tang, J.; Zhang, P.

2015, XI, 211 p. 176 illus., 160 illus. in color., Hardcover

ISBN: 978-3-662-46998-9